Journal of Sedimentary Research

Journal of Sedimentary Research, 2017, v. 87, 152–166
Research Article
DOI: http://dx.doi.org/10.2110/jsr.2017.4

PROVENANCE SIGNATURES RECORDED IN TRANSGRESSIVE SANDSTONES OF THE UPPER CRETACEOUS IBERIAN SEAWAY

LAURA GONZÁLEZ-ACEBRÓN,[1] CARLOS PÉREZ-GARRIDO,[2] RAMÓN MAS,[1] JOSÉ ARRIBAS,[3] AND JENS GÖTZE[4]

[1]*Departamento de Estratigrafía, Facultad de Ciencias Geológicas (UCM)-IGEO (CSIC), C/Jose Antonio Novais 12, 28040 Madrid, Spain*
[2]*Centro Nacional de Investigación sobre la Evolución Humana (CENIEH), Paseo Sierra de Atapuerca 3, 09002 Burgos, Spain*
[3]*Departamento de Petrología y Geoquímica, Facultad de Ciencias Geológicas (UCM)- IGEO (CSIC), C/Jose Antonio Novais 12, 28040 Madrid, Spain*
[4]*Institut für Mineralogie, Brennhausgasse 14, 0999 Frieberg, Germany*
e-mail: lgcebron@geo.ucm.es

ABSTRACT: **Maximum Mesozoic transgressions flooded many continental areas worldwide, forming a wide and shallow seaway on the Iberian Microplate during the Late Cretaceous. Several siliciclastic and mixed siliciclastic–carbonate units developed along the Iberian Massif (cratonic area) while, at the same time, epeiric carbonate platforms spanned Iberia. These siliciclastic deposits unconformably cover the Variscan basement, as well as the Permian and Triassic deposits. This study focuses on sandstone provenance in central Spain, in a transgressive, relatively quiet tectonic setting with a wide rock variety in the potential source areas. Results shown in this paper can be applied in analogue systems; transgressive sandstones often form important hydrocarbon reservoirs due to their high primary porosity. The Cretaceous siliciclastic deposits are included in four formations ranging in age from the Cenomanian to the early Coniacian. The deposits were initially of fluvial origin, followed by a coastal-tidal setting. Quantitative petrographic analysis of sandstones from these formations reveals compositional variations related to provenance and weathering degree.**

The oldest formation (Utrillas Fm.) was deposited on a paleorelief surface. Sandstone composition changes from arkosic sandstones in the depressed area (Petrofacies P1a) to younger quartzarenites when sediments were deposited on top of the paleotopographic high (Petrofacies P1b). Quartz grains in both sub-petrofacies are angular to subangular, and the framework is poorly sorted. Intense weathering conditions are deduced for Petrofacies P1b, manifested by grain infiltration, clay coatings, and the absence of plagioclase grains and alteration features on K-feldspars. All these observations have been related to wetter conditions during P1b deposition. Main source areas of the Utrillas Fm were Ordovician metasediments and orthogneisses, Permian volcanic rocks, and Triassic Buntsandstein facies.

Petrofacies 2 encompasses the three coastal-tidal formations, constituted mainly by subarkoses generally showing a subangular and poorly sorted framework. The deduced source areas are mainly associated with Variscan granitoids, pre-Ordovician schists and paragneisses, and Ordovician metasediments. Glauconite and carbonate grains support intrabasinal inputs. The low degree of sorting of this petrofacies related to a low-energy sedimentary environment produced lower values of original porosity compared to transgressive sandstone hydrocarbon reservoirs. Also, intrabasinal inputs promoted carbonate cementation and contribute to almost occlude the porosity.

INTRODUCTION

The exceptionally high global sea level during the mid and Late Cretaceous (Haq et al. 1988) is attributed to high rates of sea-floor spreading (Pitman 1978). As a consequence, wide continental areas were flooded in both Atlantic margins, forming the Western Interior Seaway on the North America plate, which reached more than 3000 km in length (Miall et al. 2008). The westernmost evidence of the maximum Mesozoic transgressions on the European margin is recorded on the Iberian microplate, forming the much smaller Iberian Seaway (600 km in length; Fig. 1), which connected the Atlantic and the Tethyan domains discontinuously during the Late Cretaceous (Alonso et al. 1994; García et al. 2004; García-Hidalgo et al. 2007).

The economic potential of transgressive sandstones as petroleum reservoirs has been outlined by several authors (e.g., Parnell 1987; Barwis 1990; Catuneanu 2006). Transgressive sands are commonly more mature both texturally and mineralogically than regressive sands, and therefore usually show high original porosity (e.g., Devine 1991; Hubbard et al. 2002; Cattaneo and Steel 2003). Transgressive processes tend to induce sediment winnowing of fines, enhancing reservoir quality (Posamentier 2002). An Upper Cretaceous example from the Western Interior Seaway is the Cardium Sandstone, an important reservoir located in Alberta (Canada), formed during the Turonian under relatively quiescent tectonic conditions (Plint et al. 1986; Miall et al. 2008).

The Upper Cretaceous sedimentary record of the Spanish Central System was characterized by relatively slow thermal subsidence (Martín-

Published Online: February 2017

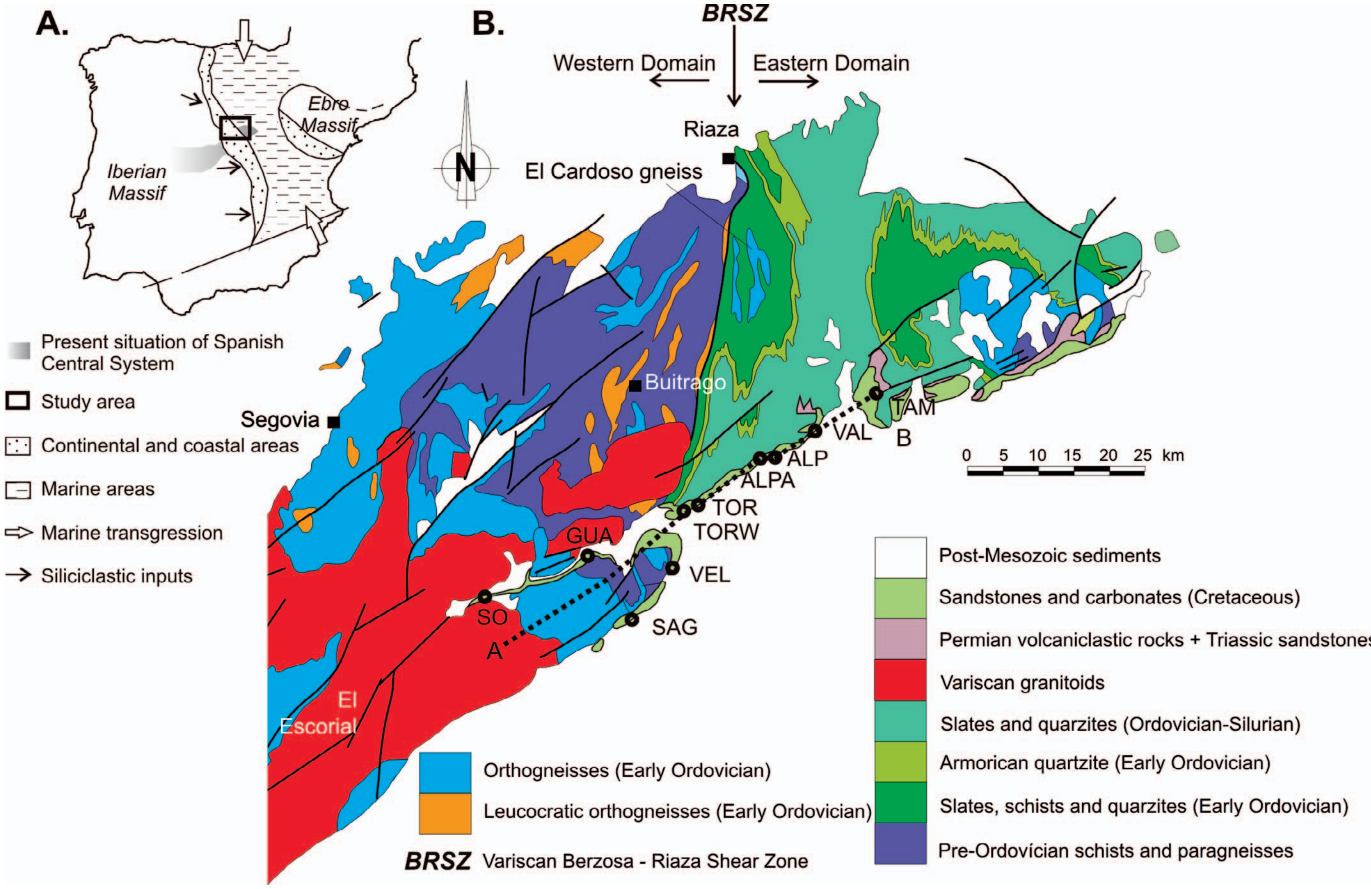

FIG. 1.—**A)** Paleogeographic map for the mid Cenomanian (~ 94 Ma) modified from Alonso et al. (1994), including the present situation of the Spanish Central System. **B)** Geological map of the southern margin of the Spanish Central System indicating the location of the stratigraphic sections. SO, Soto del Real; GUA, Guadalix de la Sierra; SAG, San Agustín de Guadalix; VEL, El Vellón; TORW, Torrelaguna (west section); TOR, Torrelaguna (east section); ALPA, Alpedrete de la Sierra (west section); ALP, Alpedrete de la Sierra (east section); VAL, Valdesotos; TAM, Tamajón. Modified from Navidad and Castiñeiras (2011).

Chivelet et al. 2002; García et al. 2004), during which siliciclastic and mixed siliciclastic–carbonate units developed along the continental areas (Iberian Massif), while epeiric carbonate platforms spanned the Iberian microplate (Alonso et al. 1994; Gil et al. 2006). The synsedimentary climate was dominantly warm and wet, due to the subtropical location of the Iberian microplate during the Late Cretaceous (approximately between 25° N and 30° N; Philip and Floquet 2000).

Sandstone petrofacies have been extensively studied in tectonically controlled sedimentary basins, such as foreland basins (e.g., Schwab 1986; DeCelles and Hertel 1989; Critelli and Le Pera 1994; White et al. 2002; Critelli et al. 2003; Garzanti et al. 2003) or rift basins (e.g., Arribas 2003, 2007, 2014; Garzanti et al. 2001; Garzanti et al. 2003; González-Acebrón et al. 2007, 2010), due to the large volumes of siliciclastic sediments produced by erosion of the active basin margins. However, provenance studies are not common in areas of relative tectonic quiescence, with lower input of siliciclastic sediments due to reduced relief. Since these settings presents low sedimentation rates, it is important to consider influence of the climate on sand transportation, deposition, and early diagenesis. Previously, composition of transgressive sandstone units has been analyzed mainly to understand their paleogeography and sequence stratigraphy (e.g., Marenssi et al. 2002; Amorosi and Zuffa 2011; Amorosi et al. 2012; Zhu and Yang 2013).

The principal aims of this paper are: (1) to document and discuss the sandstone framework composition of the Upper Cretaceous Iberian Seaway as an analog of transgressive sandstone reservoirs; (2) to evaluate the influence of postdepositional processes in the porosity evolution; (3) to determine the sandstone provenance in a geological setting of relative tectonic quiescence, to infer detailed variations in source areas and climatic conditions; and (4) to establish additional criteria to distinguish orthogneiss from granitoid source areas.

GEOLOGICAL SETTING AND STRATIGRAPHIC FRAMEWORK

The sedimentary record in the study area represents the Late Cretaceous maximum transgressions over the Iberian Massif in central Spain. The Late Cretaceous had the most extensive global sea level rise during the Mesozoic (Haq et al. 1988; Hardenbol et al. 1998), which flooded part of Iberia forming a wide and shallow seaway (Fig. 1) elongated NW–SE between the Iberian and Ebro massifs (Alonso et al. 1982; Alonso et al. 1994; García et al. 2004; García-Hidalgo et al. 2007).

The study area is located at the southern margin of the current Spanish Central System (Fig. 1), a NE–SW oriented Alpine belt crossing the Iberian Peninsula for approximately 450 km. The region is interpreted as a pop-up structure bounded by thrusts that show an opposite vergence (Warburton and Alvarez 1989; De Vicente and Muñoz-Martín 2013). The Alpine orogeny exposed the core of the chain, made up of Variscan metamorphic and igneous rocks that formerly constituted the Iberian Massif. These Variscan rocks are locally covered by Permian and Triassic siliciclastic sediments. It is important to highlight that during the deposition of the

Upper Cretaceous units the Iberian Massif was a cratonic area (Alonso et al. 1994).

In the study area the Upper Cretaceous sedimentary rocks form a NE–SW-striking outcrop belt 2–10 km wide (Fig. 1), constituting a south-dipping monocline succession or *cuesta* (Bellido et al. 1990; Bellido et al. 1991; Portero-García et al. 1990). This Upper Cretaceous succession unconformably overlies the Paleozoic basement and Triassic sedimentary rocks (Figs. 1, 2, 3).

The Variscan Berzosa-Riaza shear zone (Fig. 1) separates two different geological domains of the Iberian Massif (Escuder-Viruete et al. 1998) characterized by markedly different lithological associations, described below because they are potential source areas:

1. High-grade Western Domain, consisting of pre-Ordovician schists and paragneisses, with intercalations of orthogneisses (Fig. 1). In the westernmost area Variscan granitoids are the dominant lithology (Fig. 1). Filonian rocks are also present, including granitic calc-alkaline porphyritic dikes of highly variable thicknesses (usually 5–20 m) and long lengths (5–60 km), related to the very late Carboniferous to Early Permian magmatic event (Galindo et al. 1994; Huertas and Villaseca 1994).
2. Medium- to low-grade Eastern Domain, formed by Ordovician metasediments (slates, schists, and metaquartzites) with intercalations of orthogneisses (Fig. 1). Additionally, Permian siliciclastics (mainly conglomerates, sandstones, lutites, and volcaniclastic graywackes, Marfil and De la Peña 1987) and coals outcrop in Valdesotos area (Fig. 1, VAL). The volcaniclastic rocks show rhyolitic source composition (Marfil and De la Peña 1987). Triassic Buntsandstein facies (conglomerates, sandstones, and lutites) are also present in this area, with arkosic sandstone composition (mean $Q_{58}F_{41}R_1$—quartz, feldspar and rock fragments—Arribas et al. 1986; Ochoa and Arribas 2005).

The Upper Cretaceous succession that crops out along the southern margin of the Spanish Central System represents a Cenomanian to Maastrichtian major sedimentary cycle that has been divided into four megasequences (MS). The first two are mainly siliciclastic, and the last two are mainly carbonate (Alonso et al. 1994; García et al. 2004; Guidi et al. 2005). This study is focused on the two first siliciclastic MS and on the lower part of MS-3 (Fig. 2). The Cenomanian MS-1 (Fig. 2) consists predominantly of siliciclastic fluvial deposits, corresponding in the study area to the "Utrillas sandstones Formation." (hereafter Utrillas Fm., Figs. 2, 3, 4A, B) (Alonso and Mas 1982; Alonso et al. 1982; Guidi et al. 2004, 2005). The Utrillas Fm. is restricted to the eastern part of the study area (Fig. 3) and has variable thickness (Fig. 3), controlled by a paleotopographic step in the basement (Guidi et al. 2005).

The Utrillas Fm. passes upwards and laterally towards the NE into a mixed siliciclastic–carbonate formation, which is only 2 m thick in the study area (Fig. 3), the "Santa María de las Hoyas sandstones, lutites, and limestones Formation" (hereafter Santa María de las Hoyas Fm., Figs. 2, 3), interpreted as coastal-tidal deposits (Guidi et al. 2005).

The early Turonian–early Coniacian age MS-2 (Fig. 2) is composed of 19–32 m of glauconite-bearing sandstones and clay mudstones, with marls and sandy limestones towards the NE (Fig. 3C, D). This corresponds to the "Castro de Fuentidueña sandstones and lutites Formation," hereafter Castro de Fuentidueña Fm. (Guidi et al. 2004; 2005; Gil et al. 2004; García et al. 2004 and references therein). This formation comprises a transgressive–regressive cycle (Amorosi et al. 2012). The Castro de Fuentidueña Fm. shows a lateral transition to deeper water (mid-outer ramp) carbonate-rich deposits to the NE (VAL and TAM zone, Fig. 1) ("Picofrentes marls Formation" and "Muñecas bioclastic limestones Formation," hereafter Picofrentes Fm. and Muñecas Fm., respectively, Figs. 2, 3) (Alonso and Mas 1982; Alonso et al. 1982; García et al. 2004; Guidi et al. 2004, 2005).

The MS-3 and MS-4, of early Coniacian–late Santonian and late Santonian–Maastrichtian age, respectively (Alonso et al. 1994; Guidi et al. 2004, 2005; Gil et al. 2004; García et al. 2004), consist predominantly of inner-ramp carbonate deposits, with subordinate siliciclastic tidal units as the "Segovia sandstones and lutites Formation" (hereafter Segovia Fm., Fig. 2) (Alonso and Mas 1982; Guidi et al. 2005). The description and interpretation of the various formations is summarized in Table 1.

MATERIALS AND METHODS

Ten representative stratigraphic sections were logged in the Cretaceous sedimentary rocks (Figs. 1, 3) and 63 samples were collected for analysis. All samples were prepared as doubly polished thin sections (30 μm) impregnated with blue epoxy resin to facilitate porosity characterization.

Quantitative Petrographic Analysis

Quantitative petrographic analysis was performed on 47 selected fine- and medium-grained sandstones under conventional polarization microscope by the integrated Gazzi-Zuffa point counting method (Gazzi 1966; Zuffa 1985). This procedure is an extension of the "Gazzi-Dickinson method" (Ingersoll et al. 1984), which minimizes the compositional bias due to different grain size. Four hundred to four hundred and fifty points were counted per slide. Fifty-five petrographic categories have been distinguished, including framework, cements, and porosity (Table 2). Before point counting, carbonate-bearing thin sections were examined though cold cathodoluminescence (CITL MK4 equipment, 300–500 μA, 11–16 kV, 0.1–0.2 Torr) and later stained using alizarin-red and potassium ferricyanide (Lindholm and Finkelman 1972) to distinguish the carbonate composition of cements and framework clasts.

To assess the provenance of specific framework components, their size, morphology, and internal textures were analyzed. For quartz grains, polycrystallinity, undulosity in monocrystalline grains, and the presence of solid inclusions were studied. Porosity loss has been evaluated though the Compaction Index (ICOMPACT, Appendix 1, see Supplemental Material) following the method of Lundergard (1992). The sandstone framework composition of the studied sandstones (Table 2) were analyzed using various ternary plots (Fig. 5) and following the criteria of several authors: Dickinson et al. 1983 (QmFLt); Dickinson 1985 (QmKP); Arribas et al. 1990; and Critelli and Le Pera 1994 (RgRsRm). For definition of each parameter, see Tables 2 and 3. One petrofacies characterizes the Utrillas Fm. (P1), whereas the overlying units are grouped in a second petrofacies (P2), due to the relatively homogeneous character of their sandstones. The main compositional values and other observations of each petrofacies are summarized in Tables 3 and 4.

Quartz Cathodoluminescence

Quartz cathodoluminescence colors and internal textures of various minerals were observed on eleven carbon-coated, polished thin sections using a "hot cathode" cathodoluminescence microscope HC1-LM (cf. Neuser et al. 1995). The system was operated at 14 kV accelerating voltage and a current density of about 10 $\mu A/mm^2$. Luminescence images were captured by a Peltier-cooled digital video camera (KAPPA 961-1138 CF 20 DXC).

To interpret quartz cathodoluminescence, we have used the criteria of Ramseyer et al. (1988) and Götze et al. (2001): (1) blue to violet: plutonic quartz as well as quartz phenocrysts in volcanic rocks (often with strong zoning), and high-grade metamorphic quartz, (2) red: is exclusive of volcanic quartz, both matrix quartz and quartz phenocrysts, (3) brown: quartz from regional metamorphic rocks, (4) non luminescent or weakly

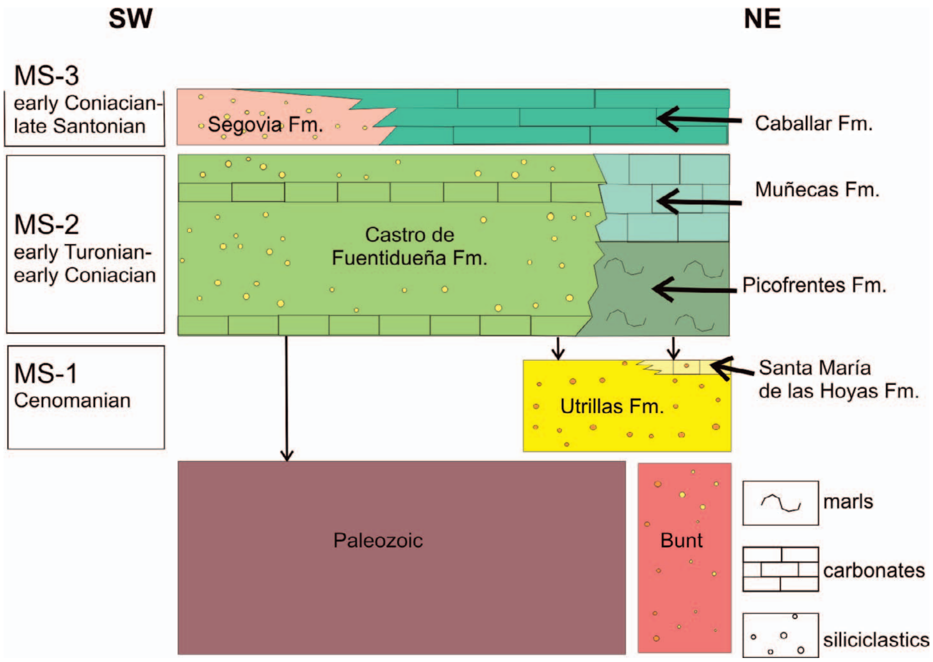

FIG. 2.—Stratigraphy of the study Cretaceous Megasequences (MS) of the southern margin of the Spanish Central System. Notice that only the lower part of MS-3 is represented. Bunt, Buntsandstein facies.

luminescent: authigenic quartz, (5) short-lived blue-green: hydrothermal and pegmatitic quartz. Metamorphic quartz that recrystallized at high temperatures (e.g., granulite) reverts to a blue luminescence color comparable to that of plutonic quartz.

Heavy Mineral Analysis

The 63–250 μm grain-size fraction from eight samples of four different stratigraphic sections (TAM, ALP, ALPA, VAL, Fig. 1) was examined for heavy mineral composition. Samples were crushed using an agate mortar, and heavy minerals were concentrated with sodium polytungstate (SPT, 2.9 g/cm^3), using 10% acetic acid to eliminate carbonates when present. The heavy minerals were split using a microsplitter and one of the splits was mounted on a slide following the procedure of Mange and Maurer (1992). More than 250 transparent grains were counted in the first suite of preparations according to the "ribbon-counting" method (Mange and Maurer 1992). The other split was prepared as a polished thin section for examination by cold cathodoluminescence (same conditions as for the carbonates; see above).

RESULTS

***Petrology of the Utrillas Fm*.** Petrofacies 1 (P1) can be divided in two sub-petrofacies. P1a occurs at the bottom of the Utrillas Fm. (Fig. 3), and occurs only in the northeasternmost sections (VAL and TAM, Figs. 1, 3). P1b is present in all sections in which the Utrillas Fm. is present (Fig. 3), corresponding with the middle and upper part of the formation.

P1a consists of angular to subangular poorly sorted arkoses, with porosities lower than 8% (Table 3). P1a mean composition is $Qm_{46}F_{53}Lt_1$ (Tables 3, 4, Fig. 5A), with K-feldspars dominating over plagioclases ($Qm_{47}K_{46}P_7$, Tables 3, 4, Fig. 5B), showing some alkali feldspars with graphic intergrowth (Fig. 6A), polycrystalline K-feldspars and microcline, and both untwinned and polysynthetically twinned plagioclases. K-feldspars present blue luminescence with brownish areas around boundaries and microfractures. Coarse-grained plutonic rock fragments are dominant, with minor arkosic sandstone (Fig. 6B), slate, and schist fragments (Table 4, Appendix 1, and Fig. 5C). Quartz appears mainly as monocrystalline grains ($Qmr_{38}Qmo_{39}Qp_{23}$, Tables 3, 4), and some scarce grains with corrosion gulfs are present. Furthermore, some quartz grains exhibit inherited quartz cements. Frequently, monocrystalline and polycrystalline quartz grains contain sillimanite needles. Most of the quartz grains have a dark blue to violet luminescence color with sparse monocrystalline dark-red luminescent quartz grains with red rims. Tourmaline, apatite, muscovite, and zircon appear as accessory minerals. Heavy mineral analysis reveals a high abundance of tourmaline (31–38%, Table 5; fresh to slightly altered, angular) and zircon (~ 10%, Table 5; fresh, both euhedral and rounded, yellow and blue cathodoluminescence grains).

Regarding diagenesis, the intergranular volume is lower than 10% (Table 3). The grains show tangential to long contacts, and cementation is less important than compaction (ICOMPACT mean 0.9, Table 3). The cements represent up to 3% of the total volume of the sandstone (Table 3). The composition of the cements is mainly quartz, feldspar, Fe-oxide, and carbonate (Appendix 1).

P1b consists of poorly sorted angular quartz rich subarkoses that change upwards to poorly sorted angular to mainly subangular quartzarenites. Porosity varies between 13 and 24% in the NE part of the study area (TAM and VAL, Fig. 1, Table 3) and is lower than 4% or almost occluded towards the central part (TOR and ALP, Fig. 1, Table 3).

The mean composition of P1b is $Qm_{96}F_4Lt_0$ (Tables 3 and 4, Fig. 5A). The scarce K-feldspars ($Qm_{96}K_4P_0$, Tables 3, 4, Fig. 5B) show luminescence features similar to the former petrofacies, but plagioclases are almost absent. Rock fragments are uncommon in comparison to P1a and are represented by coarse-grained plutonics (Fig. 5C), as well as some rhyolitic rock fragments (Fig. 6C, D) observed in the VAL section (Fig. 1). Proportions of quartz types (mean $Qmr_{29}Qmo_{44}Qp_{27}$, Tables 3, 4) are similar to those of P1a. An increase in non-undulatory monocrystalline quartz grains (Qmr) is recorded from the bottom to the top of P1b (Appendix 1). Monocrystalline quartz grains sometimes show corrosion gulfs. Frequently, P1b shows a bimodal distribution of quartz grain size, with a quartz grain population much smaller than the mean size (Fig. 6C, D). Further, quartz cathodoluminescence colors are comparable to P1a (Fig. 6E). Quartz grains with sillimanite needles, tourmaline, and zircon solid inclusions as well as abundant fluid inclusions were observed (Fig. 6F). The heavy mineral assemblage is dominated by tourmaline, staurolite (Fig. 6G), and kyanite (Table 5); the latter two are especially abundant in

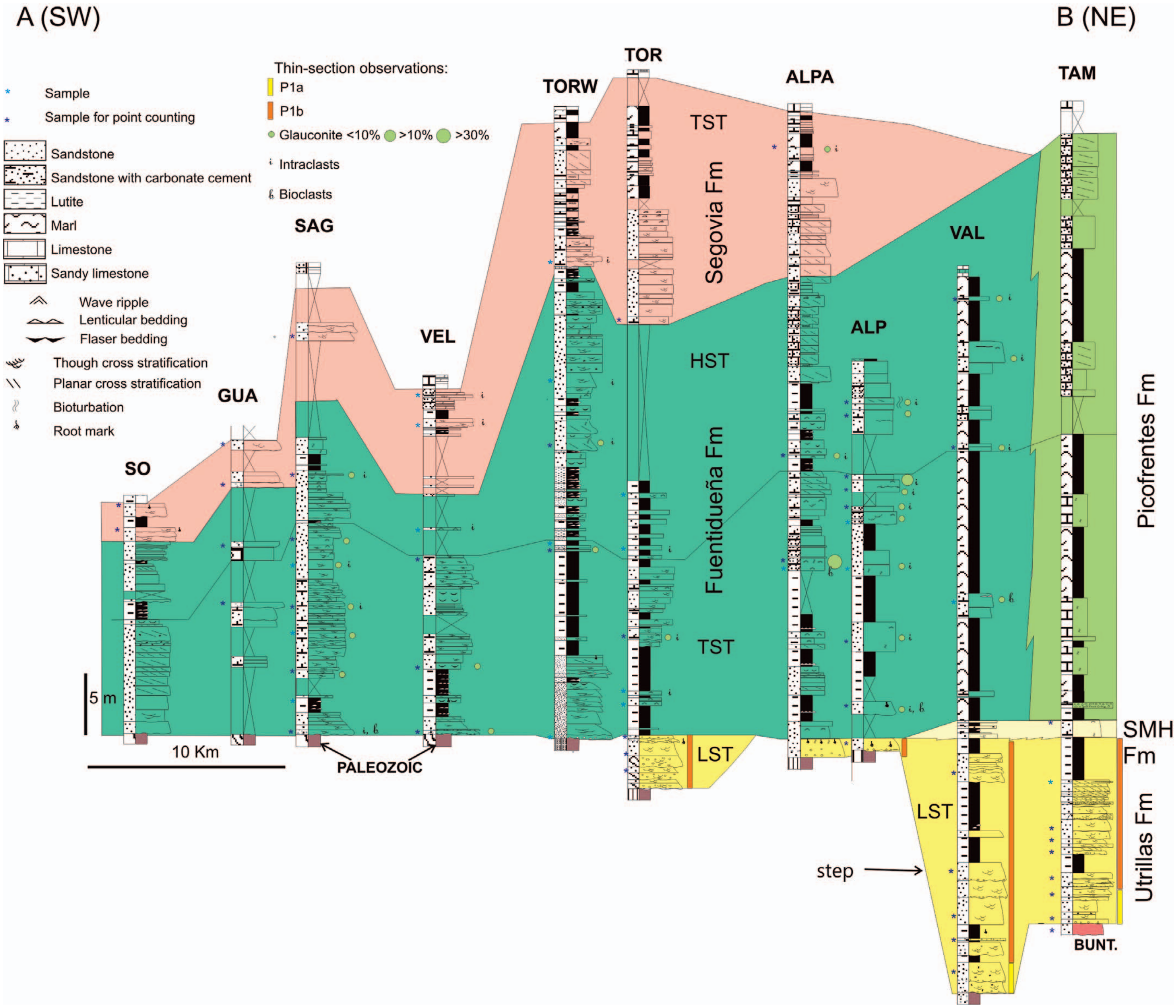

FIG. 3.—Correlation between the various sections of the southern margin of the Sierra de Guadarrama (Easter Spanish Central System). The orientation is shown in Figure 1. Sample positions are marked with an asterisk. Sections are modified from Guidi et al. (2005). For names of the stratigraphic sections see caption of Figure 1. Colors of the formations are as in Figure 2. SMH, Santa María de las Hoyas Fm. Bunt, Buntsandstein facies.

the VAL section (Fig. 1). Most staurolite grains present carbonaceous inclusions. Zircon is less abundant than in the former sub-petrofacies (< 3%) and shows yellow and blue cathodoluminescence colors.

Intergranular volume varies between 11 and 33% (Table 3). Contacts between grains are usually tangential. ICOMPACT values (mean 0.4, Table 3) indicate that cementation is more important than compaction. The cements represent 4–28% of the rock (Table 3). Kaolinite pore filling and epimatrix are rare and restricted to the VAL area (Appendix 1, Fig. 1). Illite coatings (Fig. 6C, D, G) are the dominant cement type. When these coatings are absent, the porosity is almost completely occluded by Fe-oxide and rhomboid-shaped nonferroan calcite (Fig. 6H, Appendix 1), the latter replacing part of the sandstone framework (Fig. 6H).

***Petrology of the Santa María de las Hoyas, Castro de Fuentidueña, and Segovia Fms*.** Petrofacies 2 (P2) includes all samples of Santa María de las Hoyas Fm., Castro de Fuentidueña Fm., and Segovia Fm. (Figs. 2, 3). It consists mainly of very poorly sorted angular to subangular subarkoses (Fig. 7A, B), with no clear trends in sorting or roundness (Appendix 1). The porosity is commonly occluded or quite low (1–6%, Table 3) showing only higher percentages (up to 10%) in the SAG section (Fig. 1, Table 3).

The P2 mean composition is $Qm_{83}F_{15}Lt_2$ (Tables 3, 4, Fig. 5A). Feldspars decrease generally towards the top of the sections, especially in the SW area (VEL, GUA, SAG, and SO sections, Fig. 1), where four samples are classified as quartzarenites. Nevertheless, there is not a distinct trend in most of the sections. K-feldspar dominates over plagioclase ($Qm_{83}K_{13}P_2$, Tables 2 and 3, Fig. 5B). Microcline (Fig. 7C) is observed and plagioclase is present in the same two typologies previously described in P1a.

This petrofacies is characterized by 1–6% of rounded glauconite (Fig. 7D) in most of the sections, except in the case of ALP and ALPA (Fig. 1), where this percentage varies between 2 and 16%, reaching 30% in one

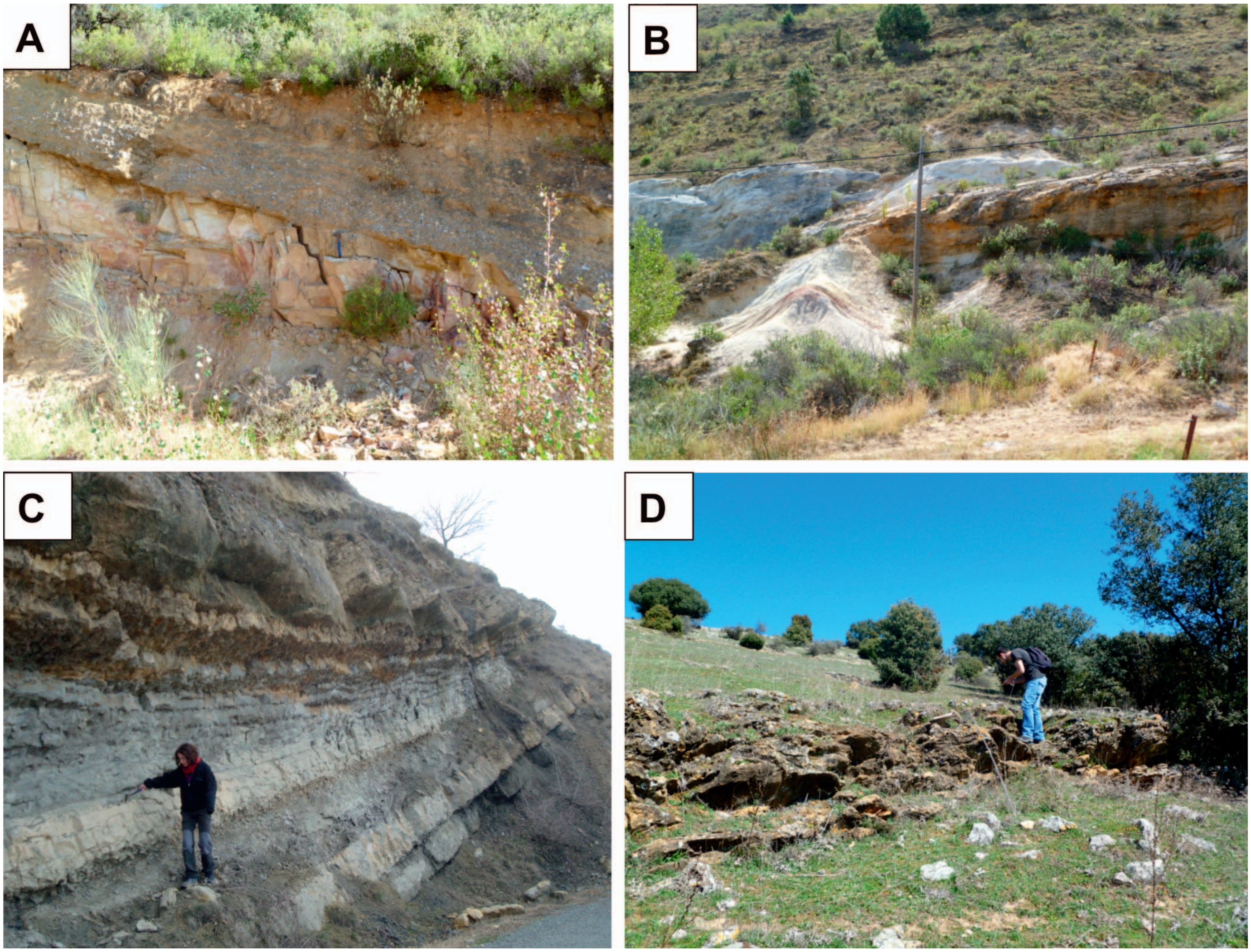

FIG. 4.—Field photographs of the study area. **A)** Unconformity between the Paleozoic and the conglomerates of the bottom of the Utrillas Fm. in San Agustín de Guadalix (SAG, Fig. 1). **B)** Fluvial channel facies of the Utrillas Fm. in Valdesotos (VAL, Fig. 1). **C)** Carbonates of the Castro de Fuentidueña Fm. in Alpedrete de la Sierra (ALP, Fig. 1). **D)** Sandstones in a coastal channel of the Castro de Fuentidueña Fm. in Guadalix de la Sierra (GUA, Fig. 1).

sample (Appendix 1). Glauconite size ranges from 50 to 300 μm and appears on different substrates, including pellets, bioclasts, phosphate fragments, and muscovite flakes. Some silicified bioclasts exist in GUA and ALP and ALPA sections (Fig. 1), including pelecypods (mainly rudist fragments) and bryozoa (Fig. 7D). Bioclasts are present mainly in the bottom part of the transgressive systems tract of the Castro de Fuentidueña Fm. (Fig. 3). Carbonate and mud intraclasts are also common, especially in the NE part of the study area (Fig. 3). The samples richest in carbonate intraclasts (~ 30–40%) show pervasive carbonate cementation and replacement (Fig. 3).

P2 has higher Qmr ($Qmr_{42}Qmo_{37}Qp_{21}$, Tables 3, 4) compared to P1b. Solid inclusions of sillimanite needles, tourmaline, and zircon are detected in quartz grains. In general, quartz has a dark blue to violet luminescent color.

Coarse-grained rock fragments with both K-feldspar and plagioclase are observed, showing microperthites (Fig. 7E). Some other coarse-grained rock fragments contain quartz, K-feldspar, biotite, muscovite and chlorite. Slate and sillimanite schist rock fragments (Fig. 7F) are present in lower proportions. Coarse porphyritic volcanic rock fragments (0.4–1.0 mm) are present in the GUA area (Figs. 1, 7G), especially at the bottom of the Castro de Fuentidueña Fm. Heavy mineral analysis indicates a significant decrease in staurolite content (1–4%, Table 5) compared to the former petrofacies. Zircon content ($< 5\%$, Table 4; yellow cathodoluminescence) is similar to that in P1b.

Concerning diagenesis, intergranular volume is between 5 and 29% (Table 3). The grains show tangential to long contacts. Intense mechanical compaction is manifested by abundant pseudomatrix (up to 10%, Appendix 1) and high ICOMPACT values (mean 0.7, Table 2). Carbonate is the dominant cement and represents highly variable portions of the rock (0–23%, Appendix 1), usually occluding the porosity. Two types of carbonate cement have been observed: A) rhomboid-shaped dolomite (red cathodoluminescence) partially or totally replaced by nonferroan calcite cement (bright orange cathodoluminescence with concentric zoning). Type A is very pervasive and usually replaces part of the sandstone framework (Fig. 7B, G) nonferroan calcite poikilotopic cements (Fig. 7A, B), which reveal concentric zoning of bright and dull luminescent orange cathodoluminescence (Fig. 7A, B).

TABLE 1.—*Summary of the studied formations based on Alonso and Mas (1982), Guidi et al. (2004, 2005), and Amorosi et al. (2012). Indicated thicknesses are only for the study area. Sequence stratigraphy refers to third-order depositional sequence. LST, lowstand systems tract; TST, transgressive systems tract; HST, highstand systems tract.*

Formation	Age	Thickness	Main Characteristics	Paleocurrents	Sedimentary Environment	Sequence Stratigraphy
Utrillas Fm.	Cenomanian	2–22 m	Finning-upwards channelized sandstone bodies, locally with basal conglomeratic lags and some interlayered lutites, with ferroan crusts and paleosols.	110° to 170°	Braided fluvial system (García Hidalgo et al. 2007) interpreted as braided alluvial plain evolving upwards to a coastal plain-bay (Atienza sequence).	LST (transgressive origin not discarded).
Santa María de las Hoyas Fm.	Cenomanian	2 m	Sandstones, lutites, and limestones		Coastal-tidal deposits	
Castro de Fuentidueña Fm.	early Turonian–early Coniacian	19–32 m	Shell-rich lag deposit (< 1 m) overlain by 10–15 m of bioturbated lutites occasionally interlayered with sandstones.		Protected bay	TST
			Amalgamated cross-bedded glauconite-bearing sandstones (~ 10 m).		Subtidal bars	
			5–20 m of lutites with interlayered sandstones showing flaser, lenticular and wavy bedding.	100° to 175° (imply coast oriented 20–30°).	Shallowing-upward sequence of intertidal origin	HST
Segovia Fm.	late Santonian–Maastrichtian	3–21 m	Sandstone bodies, some of them channelized, interlayered with mudstones with wavy and lenticular stratification.		Tidal environment	TST

TABLE 2.—*Petrographic components identified in the studied sandstone thin sections. Aside from framework and cements, porosity has also been studied.*

	FRAMEWORK	CEMENTS
	NCE	
Q	Qmr, monocrystalline quartz, extincion < 5°	Romb carbonate
	Qmo, monocrystalline quartz, extincion > 5°	Calcite
	Qm[Q], mono. quartz with inherited syntaxial overgrowth	Dolomite
	Qp2–3, polycrystalline quartz with 2 or 3 crystal units	Calcite in veins
	Qp > 3, poly. quartz with more than 3 crystal units	Quartz
	Qfrg, quartz in plutonic rock fragment	Quartz veins
	Qmi, infiltrated quartz grain	Kaolinite
	Qmg, quartz in gneiss fragment	Illite
	Qmv, volcanic quartz	Fe oxide
		K-feldspar
K	K, K-feldspar	
	Kfrg, K-feldspar in plutonic rock fragment	
	Kcao, kaolinite epimatrix on K-feldspar	
	Kcaoil, kaolinite plus illite epimatrix on K-feldspar	
	Kil, illite epimatrix on K-feldspar	
	Mc, microcline	
P	P, plagioclase	
	Ab, albite	
	Abil, illite epimatrix on albite	
	Pfrg, plagioclase in plutonic rock fragment	
L	Ch, chert	
	Sl, slate	
	Sch, schist	
	Vfr, volcanic rock fragment	
	Sdfr, sandstone fragment	
M	Ms, muscovite	
	Msfrg, muscovite in plutonic rock fragment	
	MsSch, muscovite on schist fragment	
	Bt, biotite	
CE	Lm, micritic limestone	
	Ls, esparitic limestone	
	Dm, dolomicrite	
	Ds, dolosparite	
	Fo, fossils	
NCI	Mi, mud intraclast	
	Gl, glauconite	
CI	Ci, carbonate intraclasts	
	Tu, tourmaline	
	Op, opaque	
	Es, staurolite	
	Si, sillimanite	
	Rrc, carbonate replacement (rombs)	
	Rc, carbonate replacement	
	Ps, pseudomatrix	

DISCUSSION

Utrillas Fm. The paleotopographic step in the basement (Fig. 3) probably controlled distribution of the two sub-petrofacies. P1a was only deposited from this step towards the NE (VAL and TAM, Figs. 1, 3), suggesting that this area was topographically low. Later, the unit spreads towards the SW, overstepping the paleorelief, and has a compositionally more mature sub-petrofacies (P1b).

Source Areas of P1a.—The composition of P1a plots along the Qm-F line of the QmFLt diagram (Fig. 5A). This petrofacies contains quartz with

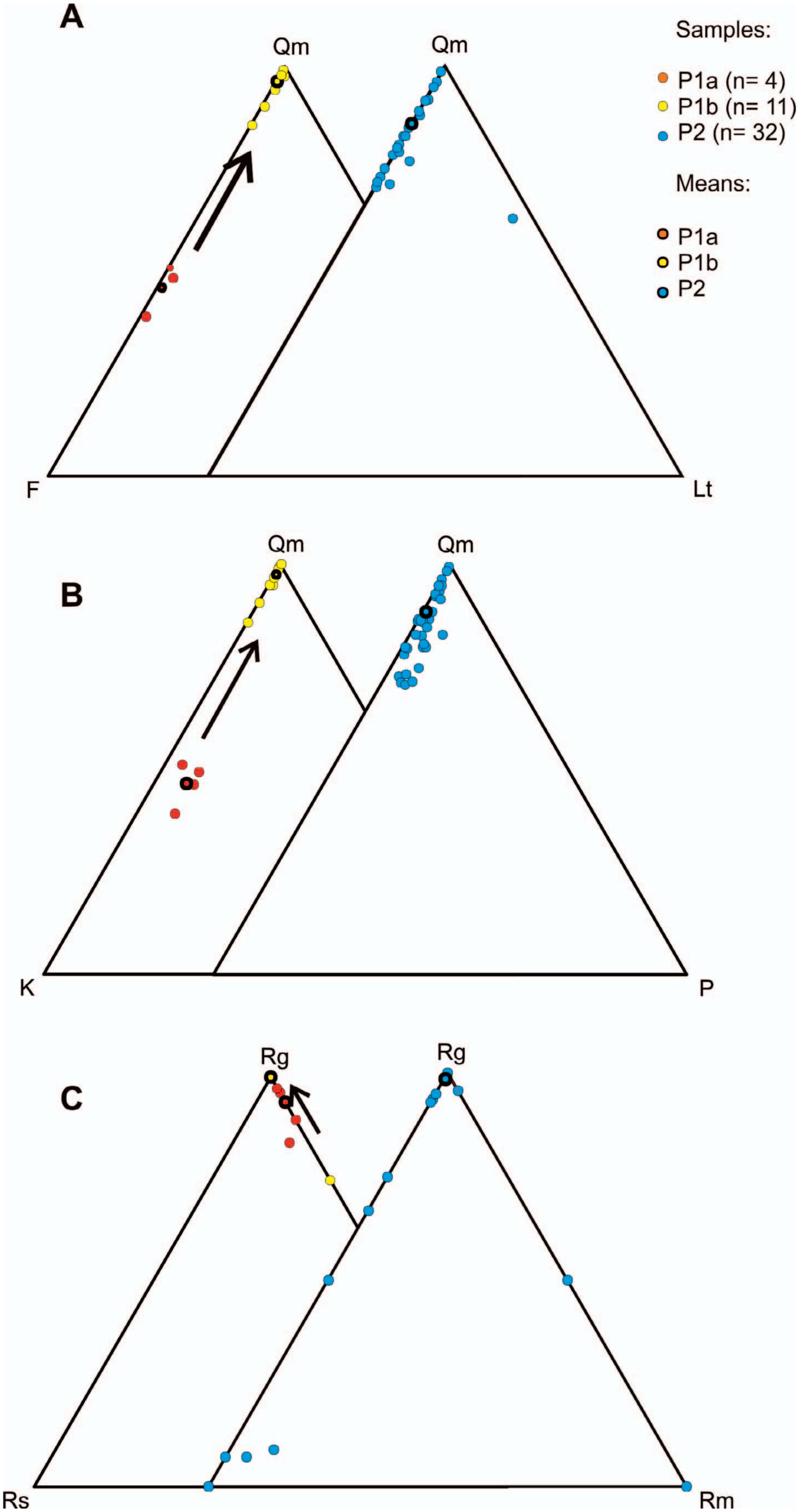

FIG. 5.—Ternary plots describing sandstone composition of the different petrofacies. **A)** QmFLt. **B)** QmKP. **C)** RgRsRm.

TABLE 3.—*Recalculated parameters used in the ternary plots. See Table 1 for abbreviations. Seq. Strati., Sequence Stratigraphy; Utrillas, Utrillas Fm.; SMH, Santa María de las Hoyas Fm.; Fuenti., Castro de Fuentidueña Fm.*

Seq. Strati.	LST	LST	LST	TST	TST	TST	HST	TST	TST	TST	LST	TST	TST	TST	TST	TST	HST	HST	TST	HST	TST	TST	TST	TST
Formation	Utrillas	Utrillas	Utrillas	Fuenti.	Segovia	Fuenti.	Fuenti.	Fuenti.	Fuenti.	Fuenti.	Utrillas	Fuenti.	Fuenti.	Fuenti.	Fuenti.	Fuenti.	Fuenti.	Fuenti.	Fuenti.	Fuenti.	Segovia	Fuenti.	Fuenti.	Fuenti.
Petrofacies	P1b	P1b	P1b	P2	P2	P2	P2	P2	P2	P2	P1b	P2	P2	P2	P2	P2	P2	P2	P2	P2	P2	P2	P2	P2
sample	TOR-1	TOR-2	TOR-5	TOR-7	TOR-10	TORW-3	TORW-5	VEL-1	VEL-2	VEL-3	ALP-1	ALP-2	ALP-3	ALP-8	ALP-9	ALP-10	ALP-11	ALP-12	ALPA-2	ALPA-3	ALPA-5	SAG-1	SAG-3	SAG-5
Qm (%)	85.8	99.2	98.1	88.5	86.8	85.5	86.4	79.5	86.3	99.3	96.8	78.2	91.5	83.1	72.9	70.9	84.8	71.0	75.0	70.3	76.5	62.7	87.8	82.7
F(%)	14.2	0.8	1.9	11.5	13.2	13.8	13.6	12.2	13.3	0.4	3.2	21.8	7.5	16.9	27.1	28.6	15.2	25.9	25.0	29.1	19.1	4.1	11.2	17.3
Lt(%)	0.0	0.0	0.0	0.0	0.0	0.6	0.0	8.3	0.4	0.4	0.0	0.0	1.0	0.0	0.0	0.5	0.0	3.1	0.0	0.6	4.3	33.2	1.0	0.0
Qm (%)	85.8	99.2	98.1	88.5	86.8	86.1	86.4	86.7	86.6	99.6	96.8	78.2	92.4	83.1	72.9	71.3	84.8	73.2	75.0	70.7	80.0	93.8	88.7	82.7
K (%)	14.2	0.8	1.9	10.9	11.0	12.7	13.6	13.3	13.0	0.4	3.2	20.6	6.9	10.1	24.5	24.8	12.5	22.6	19.1	24.1	15.8	5.4	9.4	14.6
P(%)	0.0	0.0	0.0	0.6	2.3	1.3	0.0	0.0	0.4	0.0	0.0	1.2	0.7	6.9	2.6	4.0	2.7	4.1	5.9	5.2	4.2	0.8	2.0	2.7
Qmr (%)	13.7	64.4	54.3	56.7	40.6	65.4	35.2	73.4	69.5	61.5	32.5	49.5	71.0	27.4	43.7	20.8	26.5	47.4	40.2	35.0	35.4	30.5	48.3	38.7
Qmo (%)	49.4	16.1	25.7	31.3	31.2	25.7	26.7	18.5	21.9	20.5	49.3	35.6	18.2	54.1	41.9	71.5	54.1	36.5	45.1	52.8	52.8	33.3	38.3	37.9
Qp (%)	36.9	19.5	20.0	12.0	28.2	8.8	38.2	8.1	8.6	18.0	18.2	14.9	10.8	18.5	14.4	7.6	19.4	16.1	14.7	12.2	11.8	36.2	13.3	23.4
Rg (%)	100.0	0.0	100.0	0.0	100.0	50.0	0.0	7.1	0.0	100.0	100.0	100.0	0.0	100.0	0.0	66.7	100.0	9.1	0.0	50.0	0.0	7.2	75.0	100.0
Rs (%)	0.0	0.0	0.0	0.0	0.0	50.0	0.0	92.9	0.0	0.0	0.0	0.0	0.0	0.0	0.0	33.3	0.0	81.8	0.0	0.0	100.0	88.4	25.0	0.0
Rm (%)	0.0	0.0	0.0	0.0	0.0	0.0	0.0	0.0	100.0	0.0	0.0	0.0	100.0	0.0	0.0	0.0	0.0	9.1	0.0	50.0	0.0	4.3	0.0	0.0
F/Qm	0.2	0.0	0.0	0.1	0.2	0.2	0.2	0.2	0.2	0.0	0.0	0.3	0.1	0.2	0.4	0.4	0.2	0.4	0.3	0.4	0.3	0.1	0.1	0.2
Porosity (%)	4.0	0.2	1.3	0.0	0.0	0.0	0.0	1.3	0.2	0.5	1.2	0.0	0.0	0.0	0.0	0.0	0.0	0.0	0.0	0.0	0.0	1.8	0.0	4.7
IGV (%)	21.6	28.2	20.0	9.3	4.7	18.6	19.7	9.0	19.9	23.5	11.4	7.7	2.2	8.5	16.6	7.0	6.0	18.7	7.1	6.5	18.5	15.4	11.3	14.9
Cements (%)	17.6	28.0	18.0	1.7	4.7	18.6	16.7	7.8	19.7	23.0	10.2	7.7	2.2	7.3	16.0	6.7	5.5	17.5	4.8	5.5	15.4	13.5	11.3	10.2
ICOMPACT	0.3	0.1	0.4	1.0	0.9	0.4	0.5	0.8	0.6	0.3	0.7	0.8	1.0	0.9	0.5	0.8	0.7	0.7	0.9	0.9	0.6	0.6	0.7	0.6

Seq. Strati.	TST	HST	TST	LST	LST	LST	LST	LST	LST	TST	LST	LST	LST	LST	LST	HST	HST	TST	HST	TST	TST	TST	TST
Formation	Fuenti.	Fuenti.	Segovia	Utrillas	Utrillas	Utrillas	Utrillas	Utrillas	Utrillas	SHM	Utrillas	Utrillas	Utrillas	Utrillas	Utrillas	Fuenti.	Fuenti.	Fuenti.	Fuenti.	Fuenti.	Fuenti.	Segovia	Segovia
Petrofacies	P2	P2	P2	P1a	P1a	P1a	P1b	P1b	P1b	P2	P1a	P1b	P1b	P1b	P1b	P2	P2	P2	P2	P2	P2	P2	P2
sample	SAG-7	SAG-8	SAG-9	TAM-1	TAM-2	TAM-3	TAM-4	TAM-5	TAM-6	TAM-8	VAL-1	VAL-2	VAL-3	VAL-4	VAL-5	VAL-7	VAL-9	GUA-1	GUA-2	GUA-3	GUA-4	SO-1a	SO-2
Qm (%)	80.0	80.8	96.1	45.6	38.9	48.3	90.4	97.6	95.1	78.9	51.0	94.6	97.8	99.6	96.7	71.5	80.0	91.7	82.9	91.3	98.6	94.7	88.8
F(%)	20.0	19.2	3.6	52.9	59.9	49.5	9.2	2.4	4.9	20.0	48.7	5.0	1.3	0.0	3.3	28.5	20.0	7.5	16.8	8.4	1.4	4.9	10.9
Lt(%)	0.0	0.0	0.4	1.5	1.1	2.1	0.3	0.0	0.0	1.1	0.3	0.4	0.9	0.4	0.0	0.0	0.0	0.8	0.3	0.3	0.0	0.4	0.3
Qm (%)	80.0	80.8	96.4	46.3	39.4	49.4	90.8	97.6	95.1	79.8	51.2	94.9	98.7	100.0	96.7	71.5	80.0	92.8	83.1	91.6	98.6	95.1	89.0
K (%)	15.1	15.2	3.6	45.1	52.6	42.5	9.2	2.4	4.3	19.1	45.2	5.1	1.3	0.0	3.3	22.1	19.4	6.8	15.6	6.2	1.4	4.9	11.0
P(%)	4.9	4.0	0.0	8.6	8.0	8.1	0.0	0.0	0.7	1.1	3.7	0.0	0.0	0.0	0.0	6.4	0.6	0.4	1.2	2.2	0.0	0.0	0.0
Qmr (%)	31.1	37.1	27.4	40.0	46.8	28.6	10.2	17.7	19.3	48.3	35.7	23.0	21.4	23.9	34.0	32.7	33.3	49.4	45.4	41.4	35.5	25.7	38.0
Qmo (%)	43.0	38.3	43.3	41.3	28.6	53.2	62.6	50.9	46.5	30.6	35.1	46.1	47.0	52.1	41.2	52.4	55.6	27.9	26.9	24.4	34.1	25.1	28.5
Qp (%)	25.8	24.6	29.3	18.7	24.6	18.2	27.2	31.4	34.2	21.1	29.2	30.9	31.6	23.9	24.8	14.9	11.1	22.7	27.7	34.2	30.4	49.2	33.5
Rg (%)	100.0	100.0	93.8	84.0	96.3	89.7	100.0	100.0	100.0	66.7	97.4	94.4	100.0	75.0	100.0	100.0	0.0	95.8	100.0	92.9	100.0	94.4	95.0
Rs (%)	0.0	0.0	6.3	4.0	0.0	0.0	0.0	0.0	0.0	33.3	0.0	0.0	0.0	0.0	0.0	0.0	0.0	0.0	0.0	7.1	0.0	5.6	5.0
Rm (%)	0.0	0.0	0.0	12.0	3.7	10.3	0.0	0.0	0.0	0.0	2.6	5.6	0.0	25.0	0.0	0.0	0.0	4.2	0.0	0.0	0.0	0.0	0.0
F/Qm	0.3	0.2	0.0	1.2	1.5	1.0	0.1	0.0	0.1	0.3	1.0	0.1	0.0	0.0	0.0	0.4	0.3	0.1	0.2	0.1	0.0	0.1	0.1
Porosity (%)	10.4	9.1	7.3	5.7	2.8	8.3	16.0	19.3	16.3	0.5	0.0	12.8	9.8	24.3	18.4	0.0	1.2	0.0	0.0	0.0	5.7	3.0	0.0
IGV (%)	15.4	18.2	28.8	9.0	5.4	10.0	23.8	28.4	20.0	13.8	0.2	32.5	43.2	33.3	22.6	7.0	10.4	17.2	14.8	10.4	17.1	5.1	8.6
Cements (%)	5.0	8.4	21.5	3.3	2.6	1.7	7.8	9.0	3.7	13.4	0.2	19.8	28.8	8.8	4.2	7.0	9.1	16.6	13.7	10.1	5.7	0.2	8.4
ICOMPACT	0.8	0.6	0.1	0.9	0.9	0.9	0.6	0.3	0.8	0.7	1.0	0.4	0.1	0.1	0.7	0.9	0.8	0.5	0.6	0.7	0.8	1.0	0.8

TABLE 4.—*Number of samples (n), median compositional values, and porosity ranges for each petrofacies. See Table 1 for abbreviations.*

	n	QmKLt	QmKP	Qmr Qmo Qp	Porosity
P1a	4	$Qm_{46}F_{53}Lt_1$	$Qm_{47}K_{46}P_7$	$Qmr_{38}Qmo_{39}Qp_{23}$	< 8%
P1b	11	$Qm_{96}F_4Lt_0$	$Qm_{96}K_4P_0$	$Qmr_{29}Qmo_{44}Qp_{27}$	< 24%
P2	32	$Qm_{83}F_{15}Lt_2$	$Qm_{85}K_{13}P_2$	$Qmr_{42}Qmo_{37}Qp_{21}$	< 10%

dark blue to violet luminescence, abundant coarse-grained fragments, some plagioclase and microcline, and alkali feldspars with graphic intergrowths (Fig. 6A). All these features support the erosion of orthogneisses and/or granitic rocks. Limited textural maturity (poor sorting and subangular to angular quartz grains; Appendix 1) indicates short transportation distance. This fact, together with paleocurrents (Table 1), support that orthogneisses in the cores of large Variscan anticlines (such as the current outcrop of the Cardoso orthogneiss, Fig. 1) are the source of quartz, K-feldspar (including polycrystalline deformed grains), plagioclase, and coarse-grained rock fragments. Graphic intergrowths have been described in the orthogneisses of the study area (Bellido et al. 1990). In addition, the presence of minor amounts of schist and slate rock fragments (Appendix 1) and quartz grains with sillimanite needles point to the erosion of the Ordovician metasediments of the Eastern Domain (Fig. 1). The low abundance of these types of rock fragments (Table 3, Fig. 5C) is related to the low Sand Generation Index (Palomares and Arribas 1993) of schists and slates, in comparison with other lithologies such as orthogneisses.

Sandstone inputs from the Buntsandstein facies provided quartz grains with inherited syntaxial overgrowths and arkose fragments (Fig. 6B). Finally, the presence of the dark reddish luminescent quartz with a red rim and the monocrystalline quartz grains with corrosion gulfs indicates inputs from the rhyolitic Permian rocks (Fig. 1).

P1b.—The decrease in feldspars (Fig. 5A) and feldspar-bearing coarse-grained rock fragments (Appendix 1) from P1a to P1b indicates that the latter is compositionally more mature. In addition, plagioclase is almost absent in P1b. All these facts can be related to intense weathering, which altered feldspars (especially plagioclases), probably due to weathering in warmer and wetter conditions. K-feldspars usually better resist chemical weathering than calcium plagioclases (Adams et al. 1984). Further, the brown cathodoluminescence observed in the microfractures and boundaries of the K-feldspars in this area have also been related to weathering (González-Acebrón and Götze 2012; Figs. 5–7). Chemical weathering is most efficient in areas of low relief (Dickinson et al. 1983; Dickinson 1985) such as the Iberian Massif.

This temperature rise has been proposed by other authors for the mid-Cretaceous and more specifically for the Cenomanian (Wilson and Norris 2001; Voigt et al. 2004, 2006). These studies are focused on marine environments, usually through sediment and fossil isotopic analysis. Study of sandstone weathering provides a way to evaluate climate influence in continental settings.

Although the heavy mineral assemblage in all of the studied petrofacies is biased to the highly stable minerals that resist burial diagenesis, the presence of kyanite and staurolite (Fig. 6G) in this petrofacies is a useful indicator. These minerals point to the erosion of both Variscan basement domains (Fig. 1), including pre-Ordovician metasediments (Western Domain) and Ordovician schists (Eastern Domain). Rhyolitic rock fragments (Fig. 6C, D) and quartz cathodoluminescence colors (Fig. 6E) suggest that Permian volcanic rocks continued to be eroded during the sedimentation of this petrofacies in the VAL area. The erosion of orthogneisses continued too, manifested by the presence of coarse-grained quartzofeldspathic rock fragments. The similar degree of textural immaturity of P1b (Appendix 1) compared to P1a indicates similar transportation intensity and distance.

In addition, P1b quartzarenites have some features that can be interpreted as related to infiltration as the presence of quartz grains significantly smaller than their mean grain size, and the presence of illite grain coatings (Fig. 6C, D, G). This type of coating has been related to an edaphic precursor (smectite?) as proposed by several authors (e.g., Matlack et al. 1989; Moraes and De Ros,1990, 1992), and can preserve the original porosity in sandstones (Morad et al. 2010). In our case, the coatings are located in sandstone bodies which show root traces or are located below erosional surfaces. The presence of these coatings prevents later carbonate cementation, which is very pervasive in the samples without the illite coatings (Appendix 1). Thus, the sediments may have been subject to heterogeneous diagenetic processes during the lowstand systems track, which were controlled by the presence of clay-mineral infiltration. Finally, although kaolin has been frequently described in the Utrillas Fm. (e.g., Gil et al. 2006), kaolinite pore filling and epimatrix are rare in the study area and detected only in the VAL section (Fig. 1).

***Santa María de las Hoyas, Castro de Fuentidueña, and Segovia Fms*. P2.**—This petrofacies shows a clear change in the framework composition in comparison to P1b, due to both the higher feldspar content, including plagioclase (Fig. 7A, B, C) and the intrabasinal inputs (Fig. 7D).

Glauconite is present in the Castro de Fuentidueña Fm. in both the transgressive and the highstand systems tracts, being more abundant at the upper part of the transgressive systems tract (Fig. 3). As has been highlighted by Amorosi et al. (2012), the glauconite in these sandstones is mostly allochthonous, as they are rounded and mostly concentrated in ripple troughs, coming from a coeval glauconite-bearing unit (Picofrentes marls Fm., Figs. 2, 3). Thus, the glauconite and marine bioclasts are considered to be intrabasinal (Fig. 7D).

Additionally, the presence of glauconite cements indicates some authigenic generation of glauconite. Similarly, glauconitized bioclasts (Fig. 7H) were probably glauconitized in the subarkoses of P2. This process is likely related to the large amount of allochthonous glauconite present in the petrofacies.

Most of the observed coarse-grained rock fragments are likely derived from granitoids and/or orthogneisses. The same ambiguity exists for the dark blue to violet cathodoluminescence of quartz grains. Coarse-grained rock fragments are more abundant to the west (Appendix 1). We interpret that in most cases these fragments result from the erosion of the Variscan granitoids (Fig. 1), which probably explains the increase in feldspar content in this petrofacies in comparison to P1b. Although the feldspar textures provide only qualitative provenance results (Scholonek and Augustsson 2015), the observed microperthites in feldspars from some rock fragments (Fig. 7E) can be interpreted in the same sense, since they are not commonly preserved in orthogneisses. In addition, sillimanite (Appendix 1, Table 4) and sillimanite-bearing schist fragments (Fig. 7F) support derivation from the high-grade metasediments of the Western Domain (Fig. 1). The erosion of the schists of both domains explains the presence of staurolite in the VAL, ALP, ALPA, and SO sections (Table 4, Fig. 1).

The coarse-grained porphyritic volcanic rock fragments (Fig. 7G) represent local erosion of the Permian granite porphyry dikes in the southwestern part of the study area. Considering their coarse grain size in comparison to the mean grain size of the sandstone, their well-preserved morphology (Fig. 7G), and the current position of the dike outcrops near GUA section (Fig. 1), short transportation distance can be inferred (around 3 km). In case of longer transport, rock fragments this of kind would have been disaggregated into mineral grains.

Regarding diagenetic process, this petrofacies is the one with the highest development of carbonate cement and replacement (Fig. 7A, B, C, D, E, G), probably related to the great amount in carbonate intraclasts. This

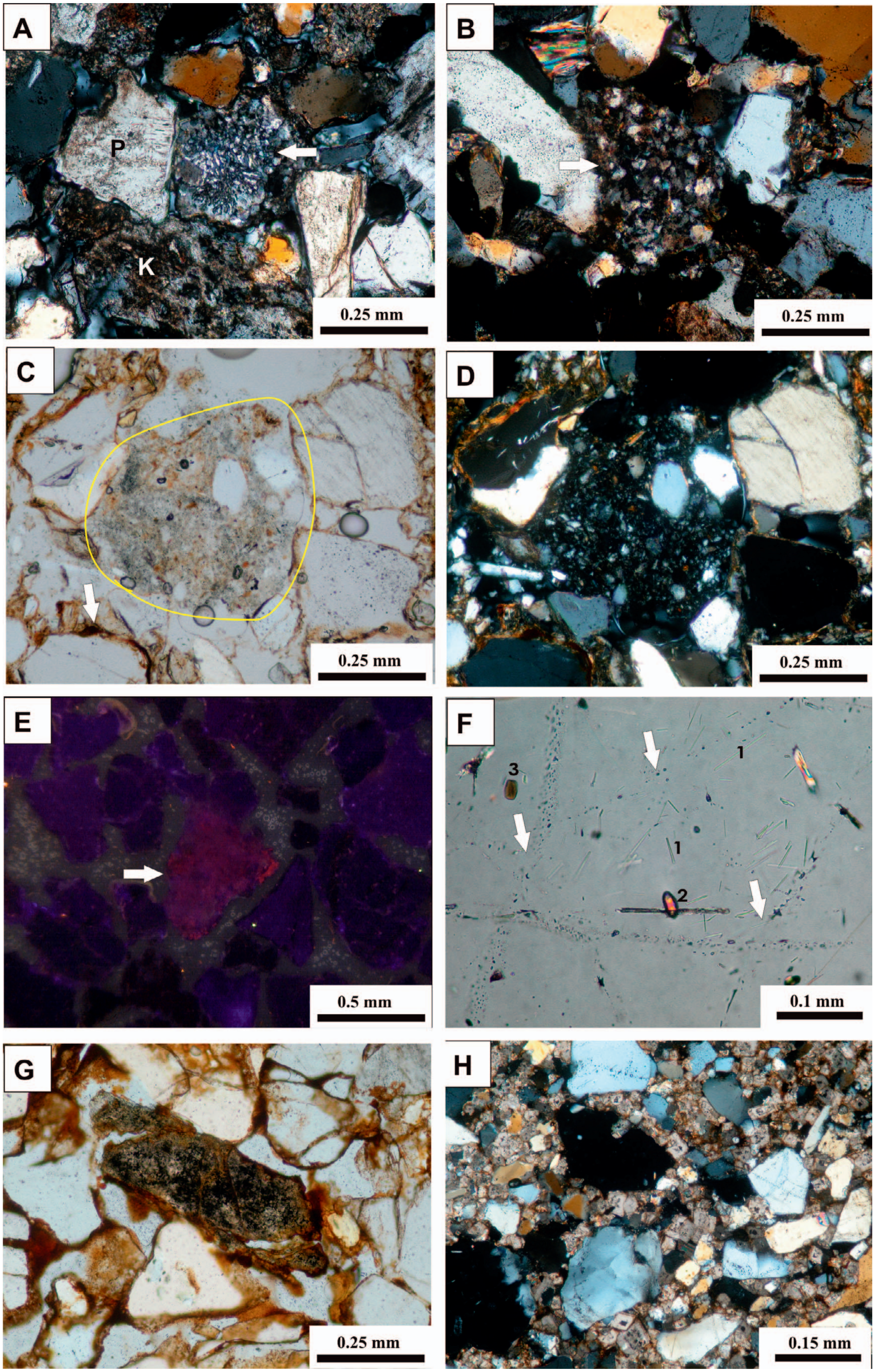

FIG. 6.—Photomicrographs of sandstone from the Utrillas Fm. **A)** Untwined plagioclase (P) and K-feldspar (K); notice another alkali feldspar with graphic intergrowth (arrow). Crossed nicols (TAM-1, P1a). **B)** Arkose sandstone fragment (arrow). Notice the abundance of monocrystalline quartz grains. Crossed nicols (TAM-1, P1a). **C**, **D)**

TABLE 5.—*Heavy mineral point counting. ZTR, ratio of zircon + tourmaline + routile* to *transparent non micaceous minerals*.

Seq. Stratigraphy	LST		LST		TST		LST		HST		TST		TST		LST		HST	
Formation	Utrillas		Utrillas		Segovia		Utrillas		Fuenti.		Fuenti.		Segovia		Utrillas		Fuenti.	
Petrofacies	P1a		P1a		P2		P1b		P2		P2		P2		P1b		P2	
Sample	TAM-2	%	TAM-3	%	SO-2	%	ALP-1	%	ALP-11	%	ALPA-2	%	ALPA-5	%	VAL-4	%	VAL-7	%
tourmaline	184	38.1	189	30.6	220	45.4	226	38.3	267	58.4	200	43.7	237.0	33.1	96	23.3	186	29.9
apatite	2	0.4	1	0.2	0	0.0	0	0.0	0	0.0	1	0.2	1.0	0.1	0	0.0	0	0.0
apatite with cement	4	0.8	0	0.0	0	0.0	0	0.0	0	0.0	0	0.0	0.0	0.0	0	0.0	0	0.0
bipyramidal zircon	19	3.9	19	3.1	3	0.6	2	0.3	1	0.2	1	0.2	4.0	0.6	0	0.0	5	0.8
subrounded zircon	9	1.9	22	3.6	10	2.1	11	1.9	3	0.7	5	1.1	12.0	1.7	2	0.5	0	0.0
rounded zircon	23	4.8	21	3.4	10	2.1	2	0.3	3	0.7	4	0.9	8.0	1.1	2	0.5	1	0.2
monazite	3	0.6	14	2.3	1	0.2	3	0.5	7	1.5	0	0.0	4.0	0.6	0	0.0	1	0.2
xenotime	1	0.2	1	0.2	0	0.0	0	0.0	0	0.0	0	0.0	0.0	0.0	0	0.0	2	0.3
staurolite	0	0.0	8	1.3	14	2.9	27	4.6	18	3.9	7	1.5	6.0	0.8	228	55.3	5	0.8
kyanite	0	0.0	0	0.0	1	0.2	2	0.3	1	0.2	0	0.0	1.0	0.1	30	7.3	0	0.0
sillimanite	0	0.0	0	0.0	2	0.4	0	0.0	1	0.2	1	0.2	0.0	0.0	0	0.0	0	0.0
rutile	11	2.3	2	0.3	7	1.4	8	1.4	11	2.4	5	1.1	29.0	4.1	6	1.5	30	4.8
anatase	16	3.3	37	6.0	13	2.7	4	0.7	18	3.9	17	3.7	27.0	3.8	0	0.0	76	12.2
brookite	6	1.2	0	0.0	1	0.2	8	1.4	2	0.4	0	0.0	12.0	1.7	1	0.2	5	0.8
muscovite	0	0.0	2	0.3	0	0.0	2	0.3	2	0.4	0	0.0	1.0	0.1	0	0.0	1	0.2
biotite	3	0.6	0	0.0	3	0.6	7	1.2	0	0.0	4	0.9	2.0	0.3	4	1.0	2	0.3
chlorite	11	2.3	0	0.0	0	0.0	0	0.0	0	0.0	0	0.0	0.0	0.0	0	0.0	0	0.0
glauconite	4	0.8	0	0.0	2	0.4	0	0.0	0	0.0	27	5.9	1.0	0.1	3	0.7	2	0.3
hornblende	1	0.2	12	1.9	0	0.0	2	0.3	0	0.0	1	0.2	0.0	0.0	0	0.0	0	0.0
garnet	0	0.0	0	0.0	0	0.0	0	0.0	0	0.0	1	0.2	0.0	0.0	0	0.0	0	0.0
carbonate	0	0.0	8	1.3	89	18.4	0	0.0	1	0.2	69	15.1	0.0	0.0	0	0.0	9	1.4
opaques	186	38.5	281	45.5	82	16.9	286	48.5	122	26.7	115	25.1	370	51.7	40	9.7	297	47.7
total	483		617		458		590		457		458		715		412		622	
ZTR	52.5		41.1		54.9		42.9		62.6		47.4		40.7		26.0		35.9	

association has been observed by other authors (Morad et al. 2010; Henares et al. 2016), particularly in transgressive systems tracts and at sequence boundaries. In our case, pervasive carbonate cementation has been observed in the transgressive lags but also along transgressive and highstand systems tracts (Appendix 1), related to dissolution of carbonate intraclasts, which are very common in both systems tracts (Fig. 3). Carbonate cement is commonly derived from diagenetic shell dissolution in the transgressive lags (Cattaneo and Steel 2003). Dolomitization and dedolomitization also played a role in decreasing the initial porosity of P2 sandstones. Thus, although transgressive sandstones are usually texturally and compositionally mature and homogeneous with high values in original porosity (e.g., Parnell 1987; Barwis 1990; Catuneanu 2006), in our case they correspond to poorly sorted angular to subangular subarkoses with important intrabasinal content and pervasive carbonate cementation. The poor sorting and subangular character of the grains are probably related to a low-energy sedimentary environment, a tide-dominated (Table 1) low-gradient margin of a shallow seaway. Further, the increase of sorting by winnowing of fines has been described mainly in shelf ridge deposits, which is not our studied case, due to long transportation during lowstands of sea level (Posamentier 2002).

Additionally, transgressive sandstones usually present better reservoir potential in the intermediate parts, because the base is rich in carbonate cements and towards the top the presence of silt and clay decreases porosity (Abbott 1985). In our case pervasive carbonate cementation is widespread (Appendix 1), and silt and clay are more abundant towards the NE (distal zones) and towards the top of the transgressive systems tracts (Fig. 3).

CONCLUSIONS

Sandstone composition and source areas associated with the maximum Mesozoic transgressions during tectonic quiescence in central Spain were studied as an analog of transgressive sandstone reservoirs. Diagenetic features were also evaluated to establish controls on porosity evolution, to improve the predictive ability in other areas with limited data coverage. Specifically, the Cenomanian fluvial Utrillas Fm. consists of lowstand-systems-tract poorly sorted sandstones with angular to subangular detrital grains in the south area of the Spanish Central System. A decrease in the fraction of feldspars from older to younger sediments is observed, with composition changing from arkoses to quartzarenites due to an increase in weathering processes. The provenance of the Utrillas Fm. appears to be dominantly from orthogneisses (Ordovician), plus sedimentary (Buntsandstein sandstones), volcanic (Permian rhyolites), and low-grade metamorphic rocks (Ordovician schists and slates). Near the top, additional input from pre-Ordovician paragneisses are inferred.

The marine and coastal sandstones of the Santa María de las Hoyas Fm. (Cenomanian, transgressive systems tract), the early Turonian–upper Cenomanian Castro de Fuentidueña Fm. (transgressive and highstand systems tract), and Segovia Fm. (transgressive systems tract) are composed of angular to subangular, very poorly sorted subarkoses, controlled by a low-energy sedimentary environment. This produced lower values of original porosity compared to transgressive-sandstone hydrocarbon reservoirs.

←
Rhyolitic rock fragment (encircled) and illite grain coatings (arrow). Parallel and crossed nicols (VAL-2, P1b). **E)** Red-luminescent quartz with red rim (arrow), surrounded by dark-blue-luminescent quartz under hot CL (VAL-5, P1b). **F)** Monocrystalline quartz containing solid inclusions of sillimanite needles (1), zircon (2), and tourmaline (3), as well as abundant fluid inclusions (arrows). Crossed nicols (TAM-6, P1b). **G)** Staurolite, monocrystalline quartz showing bimodal size distribution and illite grain coatings. Parallel nicols (VAL-3, P1b). **H)** Rhomboid-shaped nonferroan calcite (after dolomite) replacing sandstone framework. Crossed nicols (ALP-1, P1b).

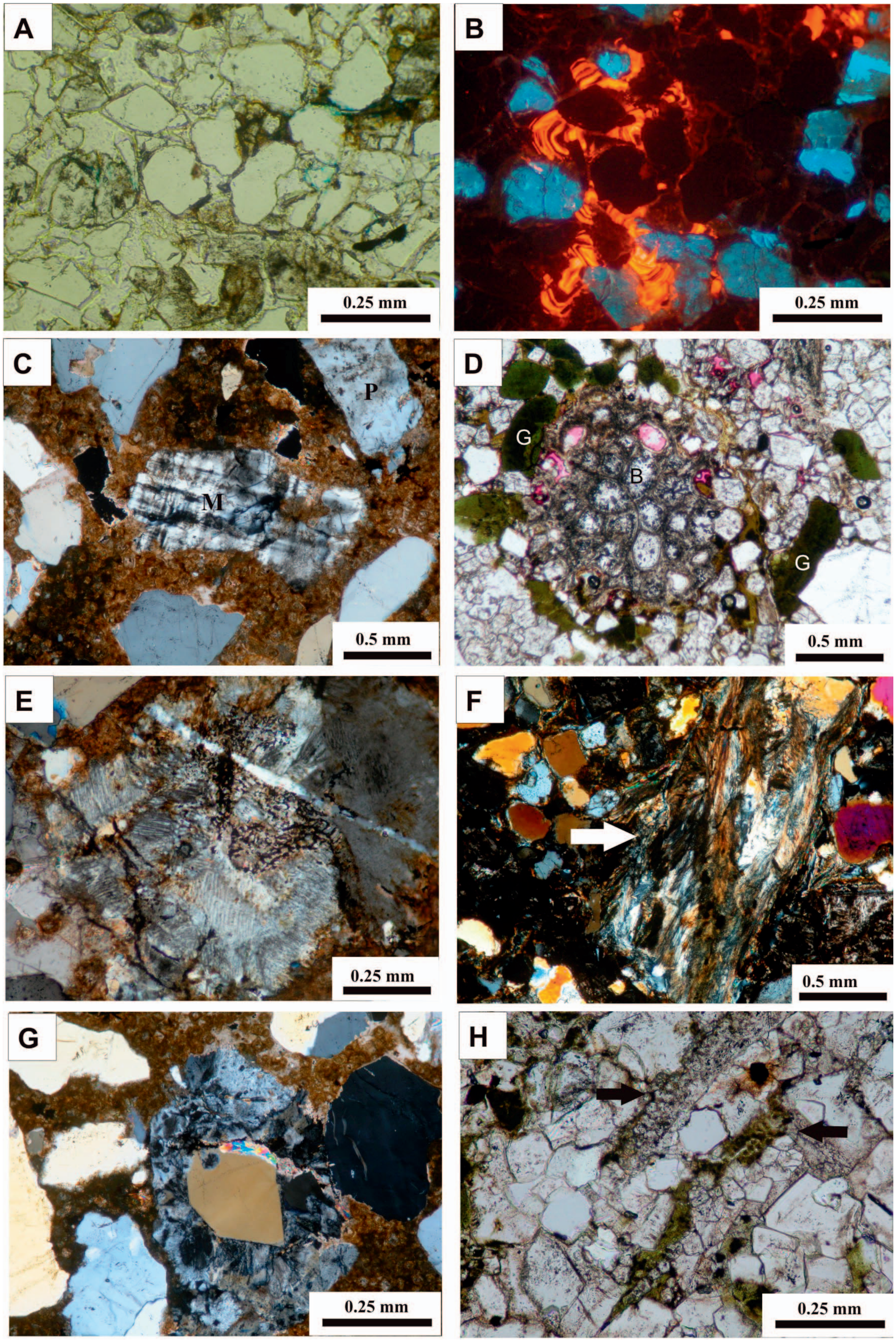

FIG. 7.—Photomicrographs of sandstone from the Castro de Fuentidueña Fm. (P2). **A)** General aspect of petrofacies 4. Parallel nicols (VEL-2). **B)** Same image as Part A under cold CL. Notice the zoned calcite cements. The blue-luminescent grains are K-feldspars, in which weathered areas exhibit dull luminescence. **C)** Microcline (M),

These formations are interpreted to have been derived from similar source areas to the Utrillas Fm., plus important contributions of the Variscan granitoids in the westernmost area. Intrabasinal inputs are inferred from the presence of glauconite grains, carbonate mud intraclasts, and marine bioclasts. Most glauconite is detrital, although some authigenic glauconite formed in these sandstones. Carbonate intraclasts promoted pervasive carbonate cementation and replacement, which typically occludes porosity.

Petrographic features, such as mineral textures (zoning, feldspar intergrowths) and other characteristics (number of subcrystal units in quartz grains, presence of rock fragments, accessory minerals, or solid inclusions) are relevant in provenance studies, especially in areas with possible plutonic and orthogneissic source rocks. In our case, sillimanite needles in quartz as well as the presence of metamorphic minerals (staurolite, sillimanite, and kyanite) have been used as qualitative indicators for the erosion of metasediments. In addition, polycrystalline K-feldspars are preferentially derived from gneissic source areas, and microperthites are typically from granites. Further, porphyritic-dike rocks generated very characteristic rock fragments containing K-feldspar and quartz, which can be considered as a provenance marker.

SUPPLEMENTAL MATERIAL

Appendix 1 is available from JSR's Data Archive: http://sepm.org/pages.aspx?pageid=229.

ACKNOWLEDGMENTS

Funding for this research was provided by the Spanish Dirección General de Investigación Científica y Técnica (DIGICYT) projects CGL2011-22709 and CGL2014-52670-P and by the research group "Sedimentary Basin Analysis" UCM 910429 of the Complutense University of Madrid, and by the Geosciences Institute (IGEO-CSIC). The authors would like to thank Mariam Barajas for her technical support. The manuscript was improved by constructive reviews by Dr. McCormick and an anonymous referee, as well as by the editor (L. Melim) and associate editor (S.L. Reeder).

REFERENCES

Abbott, W.O., 1985, The recognition and mapping of a basal transgressive sand from outcrop, subsurface, and seismic data, *in* Berg, O.R., and Woolverton, D.G., eds., Seismic Stratigraphy II: An Integrated Approach to Hydrocarbon Exploration: American Association of Petroleum Geologists, Memoir 39, p. 157–167.

Adams, A.E., Mackenzie, W.S., and Guilford, C., 1984, Atlas of Sedimentary Rocks under the Microscope: Essex, U.K., Longman Scientific and Technical, 104 p.

Alonso, A., and Mas, R., 1982, Correlación y evolución paleogeográfica del Cretácico al Norte y Sur del Sistema Central: Cuadernos de Geología Ibérica, v. 8, p. 145–166.

Alonso, A., Floquet, M., and Meléndez, A., 1982, La Meseta Norcastellana, *in* El Cretácico de España: Universidad Complutense de Madrid, p. 387–456.

Alonso, A., Floquet, M., Mas, R., and Meléndez, A., 1994, Late Cretaceous carbonate platforms: origin and evolution, Iberian Range, Spain, *in* Simó, T., Scott, R.W., and Masse, J.P., eds., Cretaceous Carbonate Platforms: American Association of Petroleum Geologists, Memoir 56, p. 297–316.

Amorosi, A., and Zuffa, G.G., 2011, Sand composition changes across key boundaries of siliciclastic and hybrid depositional sequences: Sedimentary Geology, v. 236, p. 153–163.

Amorosi, A., Guidi, R., Mas, R., and Falanga, E., 2012, Glaucony from the Cretaceous of the Sierra de Guadarrama (Central Spain) and its application in a sequence-stratigraphic context: International Journal of Earth Sciences, v. 101, p. 415–427.

Arribas, J., Marfil, R., and De la Peña, J.A., 1986, Provenance of Triassic feldspathic sandstones in the Iberian Range (Spain): Journal of Sedimentary Petrology, v. 55, p. 864–868.

Arribas, J., Gómez-Gras, D., Rossel, J., and Tortosa, A., 1990, Estudio comparativo de las areniscas paleozoicas y triásicas de la isla de Menorca: evidencias de procesos de reciclado: Sociedad Geológica de España, Revista, v. 3, p. 105–116.

Arribas, J., Alonso, A., Mas, R., Tortosa, A., Rodas, M., Barrenechea, J.F., Alonso-Azcarate, J., and Artigas, R., 2003, Sandstone petrography of continental depositional sequences of an intraplate rift basin: Western Cameros Basin (North Spain): Journal of Sedimentary Research, v. 73, p. 309–327.

Arribas, J., Ochoa, M., Mas, R., Arribas, M.E., and González-Acebrón, L., 2007, Sandstone petrofacies in the northwestern sector of the Iberian Basin: Journal of Iberian Geology, v. 33, p. 191–206.

Arribas, J., González-Acebrón, L., Omodeo-Salè, S., and Mas, R., 2014, The influence of the provenance of arenite in its diagenesis in the Cameros Rift Basin, *in* Scott, R.A., Smyth, H.R., Morton, A.C., and Richardson, N., eds., Sediment Provenance Studies in Hydrocarbon Exploration and Production: Geological Society of London, Special Publication 386, p. 63–73.

Barwis, J.H., 1990, Flood-tidal delta reservoirs, Medora–Dickinson Trend, North Dakota, *in* Barwis, J.H., McPherson, J.G., and Studlick, R.J.J., eds., Sandstone Petroleum Reservoirs: Berlin, Springer-Verlag, p. 389–412.

Bellido, F., Casquet, C., González Lodeiro, F., Martín Parra, L.M., Martínez-Salanova, J., Navidad, M., and Del Olmo, A., 1990, Mapa Geológico de España: hoja 509 (Torrelaguna), Instituto Tecnológico Geominero de España, Madrid, scale 1:50.000.

Bellido, F., Casquet, C., Escuder, J., Klein, E., Navidad, M., Peinado, M., and Del Olmo, A., 1991, Mapa Geológico de España: Instituto Tecnológico Geominero de España, Madrid, hoja 484 (Buitrago de Lozoya), scale 1:50.000.

Catuneanu, O., 2006, Principles of Sequence Stratigraphy: Amsterdam, Elsevier, 375 p.

Cattaneo, A., and Steel, R.J., 2003, Transgressive deposits: a review of their variability: Earth-Science Reviews, v. 62, p. 187–228.

Critelli, S., and Le Pera, E., 1994, Detrital modes and provenance of Miocene sandstones and modern sands of the Southern Apennines thrust-top basins, Italy: Journal of Sedimentary Research, v. 64, p. 824–835.

Critelli, S., Arribas, J., Le Pera, E., Tortosa, A., Marsaglia, K.M., and Latter, K.K., 2003, The recycled orogenic sand provenance from an uplifted thrust belt, Betic Cordillera, Southern Spain: Journal of Sedimentary Research, v. 73, p. 72–81.

DeCelles, P.G., and Hertel, F., 1989, Petrology of fluvial sands from the Amazonian foreland basin, Peru and Bolivia: Geological Society of America, Bulletin, v. 101, p. 1552–1562.

De Vicente, G., and Muñoz-Martín, A., 2013, The Madrid Basin and the Central System: A tectonostratigraphic analysis from 2D seismic lines: Tectonophysics, v. 602, p. 259–285.

Devine, P.E., 1991, Transgressive origin of channeled estuarine deposits in the Point Lookout Sandstone, northwestern New Mexico: a model for Upper Cretaceous, cyclic regressive parasequences of the US Western Interior: American Association of Petroleum Geologists, Bulletin, v. 75, p. 1039–1063.

Dickinson, W.R., Beard, L.S., Barkenrigge, G.R., Erjavec, J.L., Ferguson, R.C., Inman, K.F., Knepp, R.A., Lindberg, F.A., and Ryberg, P.T., 1983, Provenance of North America Phanerozoic sandstones in relation to tectonic setting: Geological Society of America, Bulletin, v. 94, p. 222–235.

Dickinson, W.R., 1985, Interpreting provenance relations from detrital modes of sandstones, *in* Zuffa, G.G., ed., Provenance of Arenites: Dordrecht, The Netherlands, Reidel, p. 333–361.

Escuder-Viruete, J., Hernáiz-Huerta, P.P., Valverde-Vaqueroc, P., Rodríguez-Fernández, R., and Dunning, G., 1998, Variscan syncollisional extension in the Iberian Massif: structural, metamorphic and geochronological evidence from the Somosierra sector of the Sierra de Guadarrama (Central Iberian Zone, Spain): Tectonophysics, v. 290, p. 87–109.

Galindo, C., Huertas, M.J., and Casquet, C., 1994, Cronología Rb-Sr y K-Ar de diques de la Sierra de Guadarrama (Sistema Central Español): Geogaceta, v. 16, p. 23–26.

García, A., Mas, R., Segura, M., Carenas, B., García-Hidalgo, J.F., Gil, J., Alonso, A., Aurell, M., Bádenas, B., Benito, M.I., Meléndez, A., and Salas, R., 2004, Segunda fase de postrifting: Cretácico Superior, *in* Vera, J., ed., Geología de España: Sociedad Geológica de España, Instituto Geológico y Minero de España, p. 510–522.

García-Hidalgo, J.F., Gil, J., Segura, M., and Dominguez, C., 2007, Internal anatomy of a mixed siliciclastic–carbonate platform: the late Cenomanian–middle Turonian at the southern margin of Spanish Central System: Sedimentology, v. 54, p. 1245–1271.

Garzanti, E., Vezzoli, G., Andò, S., and Castiglioni, G., 2001, Petrology of rifted-margin sand (Red Sea and Gulf of Aden, Yemen): Journal of Geology, v. 109, p. 277–297.

Garzanti, E., Andò, S., Vezzoli, G., and Dell'Era, D., 2003, From rifted margins to foreland basins: investigating provenance and sediment dispersal across desert Arabia (Oman, U.A.E.): Journal of Sedimentary Research, v. 73, p. 572–588.

←

plagioclase (P), and monocrystalline quartz grains. Notice the pervasive carbonate cementation and replacement of sandstone framework. Crossed nicols (GUA-1). **D)** Silicified bryozoan (B) and glauconite (G) grains. Notice the presence of nonferroan calcite cement in the bryozoan's zoecias (pink stained). Parallel nicols (ALPA-2). **E)** Microperthite textures in a coarse-grained rock fragment. Notice a thin quartz vein crossing the fragment. Crossed nicols (GUA-1). **F)** Schist fragment with sillimanite. Crossed nicols (SAG-1). **G)** Coarse porphyritic rock fragment. Crossed nicols (GUA-1). **H)** Glauconized bioclasts (arrows). Notice the pervasive carbonate replacement of the sandstone framework. Parallel nicols (ALPA-2).

Gazzi, P., 1966, Le arenarie del flysch sopracretaceo dell'Appenino modenese; correlazioni con il flysch di Monghidoro: Mineralogica Petrografica Acta, v. 12, p. 69–97.

Gil, J., Carenas, B., Segura, M., García-Hidalgo, J.F., and García, A., 2004, Revisión y correlación de las unidades litoestratigráficas del Cretácico Superior en la región central y oriental de España: Sociedad Geológica de España, Revista, v. 17, p. 249–266.

Gil, J., García-Hidalgo, J.F., Segura, M., García, A., and Carenas, B., 2006, Stratigraphic architecture, palaeogeography and sea-level changes of a third order depositional sequence: the late Turonian–early Coniacian in the northern Iberian Ranges and Central System (Spain): Sedimentary Geology, v. 191, p. 191–225.

González-Acebrón, L., and Götze, J., 2012, Cathodoluminiscence of feldspars and carbonate in sedimentary rocks, *in* Silvester, P., ed., Quantitative Mineralogy and Microanalysis of Sediments and Sedimentary Rocks: Mineralogical Association of Canada, Short Course, v. 42, p. 75–98.

González-Acebrón, L., Arribas, J., and Mas, R., 2007, Provenance of fluvial sandstones at the start of late Jurassic–early Cretaceous rifting in the Cameros Basin (N. Spain): Sedimentary Geology, v. 202, p. 138–157.

González-Acebrón, L., Arribas, J., and Mas, R., 2010, Sand provenance and implications for paleodrainage in a rifted basin: the Tera Group (N. Spain): Journal of Iberian Geology, v. 36, p. 179–184.

Götze, J., Plötze, M., and Habermann, D., 2001, Origin, spectral characteristics and practical applications of the cathodoluminescence (CL) of quartz: a review: Mineralogy and Petrology, v. 71, p. 225–250.

Guidi, R., Mas, R., and Sarti, G., 2004, Analisi di facies dei depositi terrigeni del Cretaceo superiore del versante sud della "Sierra de Guadarrama" (Madrid, Spagna centrale): dati preliminari: Societa Toscana di Scienze Naturali di Pisa Memorie, Atti, Serie A, v. 109, p. 69–76.

Guidi, R., Mas, R., and Sarti, G., 2005, La sucesión sedimentaria siliciclástica del Cretácico Superior del borde Sur de la Sierra de Guadarrama (Madrid, España Central): Análisis de facies y reconstrucción paleoambiental: Sociedad Geológica de España, Revista, v. 18, p. 99–111.

Haq, B.U., Hardenbol, J., and Vail, P.R., 1988, Mesozoic and Cenozoic chronostratigraphy and cycles of sea level change, *in* Wilgus, C.K., Hastings, B.S., Kendall, C.G.T.C., Posamentier, H., Ross, C.A., and Van Wagoner, J.C., eds., Sea Level Changes: An Integrated Approach: SEPM, Special Publication 42, p. 71–108.

Hardenbol, J., Thierry, J., Farley, M.B., Jacquin, T., De Gracianski, P.C., and Vail, P., 1998, Mesozoic and Cenozoic sequence chronostratigraphic framework of European basins, *in* De Gracianski, P.C., Hardenbol, J., and Vail, P., eds., Mesozoic and Cenozoic Sequence Stratigraphy of European Basins: SEPM, Special Publication 60, p. 3–13.

Henares, S., Arribas, J., Cultrone, G., and Viseras, C., 2016, Muddy and dolomitic rip-up clasts in Triassic fluvial sandstones: origin and impact on potential reservoir properties (Argana Basin, Morocco): Sedimentary Geology, v. 339, p. 218–233.

Hubbard, S.M., Gingras, M.K., Pemberton, S.G., and Thomas, M.B., 2002, Variability in wave-dominated estuary sandstones: implications on subsurface reservoir development: Bulletin of Canadian Petroleum Geology, v. 50, p. 118–137.

Huertas, M.J., and Villaseca, C., 1994, Les derniers cycles magmatiques posthercyniens du sistème central espagnol: les essaims filoniens calco-alcalins: Schweiz: Swiss Bulletin of Mineralogy and Petrology, v. 74, p. 383–401.

Ingersoll, R.V., Bulard, T.F., Ford, R.L., Grimm, J.P., Pickle, J.D., and Sares, S.W., 1984, The effect of grain size on detrital modes: a text of the Gazzi-Dickinson point-counting method: Journal of Sedimentary Petrology, v. 54, p. 103–116.

Lindholm, R.C., and Finkelman, R.B., 1972, Calcite staining: semiquantitative determination of ferrous iron: Journal of Sedimentary Petrology, v. 42, p. 239–245.

Lundergard, P.D., 1992, Sandstone porosity loss. A "big picture" view of the importance of compaction: Journal of Sedimentary Petrology, v. 62, p. 250–260.

Mange, M.A., and Maurer, H.F.W., 1992, Heavy minerals in colour: London, Chapman and Hall, 147 p.

Marenssi, S.A., Net, L.I., and Santillana, S.N., 2002, Provenance, environmental and paleogeographic controls on sandstone composition in an incised-valley system: the Eocene La Meseta Formation, Seymour Island, Antarctica: Sedimentary Geology, v. 150, p. 301–321.

Marfil, R., and De la Peña, J.A., 1987, Estudio petrológico de las series posthercínicas (Carbonífero–Pérmico?) en el borde del Sistema Central (Guadalajara): Cuadernos de Geología Ibérica, v. 11, p. 515–534.

Martín-Chivelet, J., Berástegui, X., Rosales, I., Vilas, L., Vera, J.A., Caus, E., Gräfe, K.-U., Mas, R., Puig, C., Segura, M., Robles, S., Floquet, M., Quesada, S., Ruiz-Ortiz, P.A., Fregenal-Martínez, M.A., Salas, R., Arias, C., García, A., Martín-Algarra, A., Meléndez, M.N., Chacón, B., Molina, J.M., Sanz, J.L., Castro, J.M., García-Hernández, M., Carenas, B., García-Hidalgo, J., Gil, J., and Ortega, F., 2002, Cretaceous, *in* Gibbons, W., and Moreno, T., eds., The Geology of Spain: The Geological Society of London, p. 255–292.

Matlack, K.S., Houseknecht, D.W., and Applin, K.R., 1989, Emplacement of clay into sand by infiltration: Journal of Sedimentary Petrology, v. 59, p. 77–87.

Miall, A.D., Catuneanu, O., Vakarelov, B.K., and Post, R., 2008, The Western Interior Basin, *in* Miall, A.D., ed., Sedimentary Basins of the World, Volume 5: Sedimentary Basins of the United States and Canada: Amsterdam, Elsevier, p. 330–358.

Morad, S., Al-Ramadan, K., Ketzer, J.M., and de Ros, L.F., 2010, The impact of diagenesis on the heterogeneity of sandstone reservoirs: a review of the role of depositional facies and sequence stratigraphy: American Association of Petroleum Geologists, Bulletin, v. 94, p. 1267–1309.

Moraes, M., and de Ros, L.F., 1990, Infiltrated clays in fluvial Jurassic sandstones of Recôncavo Basin, northeastern Brazil: Journal of Sedimentary Petrology, v. 60, p. 809–819.

Moraes, M., and de Ros, L.F., 1992, Depositional, infiltrated, and authigenic clays in fluvial sandstones of the Jurassic Sergi Formation, Recôncavo Basin, northeastern Brazil, *in* Houseknecht, D.W., and Pittman, E.W., eds., Origin, Diagenesis, and Petrophysics of Clay Minerals in Sandstones: SEPM, Special Publication 47, p. 197–208.

Navidad, M., and Castiñeiras, P., 2011, Early Ordovician magmatism in the Northern Central Iberian Zone (Iberian Massif): new U-Pb (SHRIMP) ages and isotopic Sr-Nd data, *in* Gutiérrez-Marco, J.C., Rábano, I., and García-Bellido, D., eds., Ordovician of the World: Cuadernos del Museo Geominero, v. 14, p. 391–398.

Neuser, R.D., Bruhn, F., Götze, J., Habermann, D., and Richter, D.K., 1995, Kathodolumininneszenz: Methodik und Anwendung: Zentralblatt für Geologie und Paläontologie, Teil I, H, 1, p. 287–306.

Ochoa, M., and Arribas, J., 2005, Diagenetic paths in the margin of a Triassic Basin: NW zone of the Iberian Chain, Spain: International Journal of Earth Sciences, v. 94, p. 256–266.

Palomares, M., and Arribas, J., 1993, Modern stream sands from compound crystalline sources: composition and sand generation index, *in* Johnsson, M.J., and Basu, A., eds., Processes Controlling the Composition of Clastic Sediments: Geological Society of America, Special Paper 284, p. 313–322.

Parnell, J., 1987, Secondary porosity in hydrocarbon-bearing transgressive sandstones on an unstable Lower Palaeozoic continental shelf, Welsh Borderland, *in* Marshall, J.D., ed., Diagenesis of Sedimentary Sequences: Geological Society of London, Special Publication 36, p. 297–312.

Philip, J., and Floquet, M., 2000, Late Cenomanian (94.7–935 Ma), *in* Dercourt, J., Gaetani, M., Vrielynck, B., Barrier, E., Biju-Duval, B., Brunet, M.F., Cadet, J.P., Crasquin, S., and Sandulescu, M., eds., Peri-Tethys Palaeogeographical Atlas: Commission for the Geological Map of the world, Paris.

Pitman, W.C., III, 1978, Relationship between eustasy and stratigraphic sequences of passive margins: Geological Society of America, Bulletin, v. 89, p. 1389–1403.

Plint, A.G., Walker, R.G., and Bergman, K.M., 1986, Cardium Formation 6: stratigraphic framework of the Cardium in subsurface: Bulletin of Canadian Petroleum Geology, v. 34, p. 213–225.

Portero-García, J.M., Aznar Aguilera, J.M., Pérez González, A., and González Lodeiro, F., 1990, Mapa Geológico de España: hoja 485 (Valdepeñas de la Sierra): Instituto Tecnológico Geominero de España, Madrid, scale 1:50.000.

Posamentier, H.W., 2002, Ancient shelf ridges: a potentially significant component of the transgressive systems tract: case study from offshore northwest Java: American Association of Petroleum Geologists, Bulletin, v. 86, p. 75–106.

Ramseyer, K., Baumann, J., Matter, A., and Mullis, J., 1988, Cathodoluminescence colors of alpha quartz: Mineralogical Magazine, v. 52, p. 669–677.

Schwab, F., 1986, Sedimentary "signatures" of foreland basin assemblages: real or counterfeit? *in* Allen, P.A., and Homewood, P., eds., Foreland Basins: International Association of Sedimentologists, Special Publication 8, p. 395–410.

Scholonek, C., and Augustsson, C., 2015, Can cathodoluminescence of feldspar be used as provenance indicator?: Sedimentary Geology, v. 336, p. 36–45.

Voigt, S., Gale, A.S., and Flögel, S., 2004, Midlatitude shelf seas in the Cenomanian–Turonian greenhouse world: temperature evolution and North Atlantic circulation: Paleoceanography, v. 19, no. PA4020, p. 1–17.

Voigt, S., Gale, A.S., and Flögel, S., 2006, Sea-level change, carbon cycling and palaeoclimate during the Late Cenomanian of northwest Europe; an integrated palaeoenvironmental analysis: Cretaceous Research, v. 27, p. 836–858.

Warburton, J., and Álvarez, C., 1989, A thrust tectonic interpretation of the Guadarrama mountains, Spanish Central System: Asociación Geológica Geoforum Española del Petróleo, p. 147–157.

White, N.M., Pringle, M., Garzanti, E., Bickle, M., Najman, Y., Chapman, H., and Friend, P., 2002, Constraints on the exhumation and erosion of the High Himalayan Slab, NW India, from foreland basin deposits: Earth and Planetary Science Letters, v. 195, p. 29–44.

Wilson, P., and Norris, R.D., 2001, Warm tropical ocean surface and global anoxia during the mid-Cretaceous period: Nature, v. 412, p. 425–429.

Zhu, L., and Yang, W., 2013, Petrographic characteristics of maximum-transgressive and regressive deltaic sandstones of Upper Pennsylvanian (Virgilian) Oread Cyclothem, NE Oklahoma [Abstract]: Geological Society of America, Abstracts with Programs, v. 44, p. 17.

Zuffa, G.G., 1985, Optical analyses of arenites: influence of methodology on compositional results, *in* Zuffa, G.G., ed., Provenance of Arenites: Dordrecht, The Netherlands, Reidel, p. 165–189.

Received 29 March 2016; accepted 12 November 2016.